Ethanolysis of N-substituted norbornane epoxyimides: Discovery of diverse pathways depending on substituent's character†

Tetyana Petrova,[a,b] Igor Tarabara,[a] Vitaliy Palchikov,[a] Liliya Kasyan,[a] Dmytro Kosenkov,[b] Sergiy Okovytyy,[a] Leonid Gorb,[b,c] Svetlana Shishkina,[d] Oleg Shishkin[d] and Jerzy Leszczynski*[b]

Received 1st September 2009, Accepted 16th February 2010
First published as an Advance Article on the web 9th March 2010
DOI: 10.1039/b917850c

Combined experimental and theoretical studies have been carried out to investigate the transformations of the epoxyimides of norbornane into heterocyclic compounds. We established that interaction of the aryl-substituted epoxyimides of norbornane with sodium ethoxide results in the formation of new heterocyclic compounds in preparatively useful yields and with complete regioselectivity. The reactions of epoxyimides, containing aryl electron-donor substituents, result in the formation of *endo*-9-carbamoyl-*exo*-2-hydroxy-5-oxo-4-oxatricyclo[4.2.1.$0^{3,7}$]nonanes, while in the case of the absence of an aryl electron-donor group or the presence of aryl electron-withdrawing group in the epoxyimide, *exo*-2-hydroxy-5-oxo-4-azatricyclo[4.2.1.$0^{3,7}$]nonan-*endo*-9-carboxylic acids were obtained as products of the ethanolysis reaction. Unexpectedly, the ethanolysis of alkyl-substituted epoxyimides leads to dihydroxyimide formation as the major product. In order to understand the vital role of the imide substituent, a systematic theoretical DFT study at the PCM/B3LYP/6-31+G(d) level was carried out. We found that substituents at the nitrogen atom of epoxyimides exerted remarkable effects on the regioselectivity in the ethanolysis reaction, based on the solvent effects and intramolecular electronic interactions. Particularly, the preference for the formation of dihydroxyimides over heterocyclic systems for alkyl derivatives might be explained by kinetic stability of the formed acetal intermediate over the competitive epoxyamido acid intermediate. The above results provide a convenient and efficient method for predicting the structures of heterocyclic systems formed under basic ethanol conditions depending on the substituent on the nitrogen atom of the norbornane epoxyimides.

Introduction

Over the years, norbornenes have received considerable attention because they display a wide range of biological activities.[1] For example, they possess the following types of pharmacological activities: cytotoxic,[1i,1l] psychotropic,[1m] anticancer,[1l,1n,1o] anticonvulsant[1p] and antidepressant,[1q] and in addition, have been used for the treatment of diseases of the central nervous system,[1m,1r] blood circulatory system, particularly, as antiarrhythmic,[1s,1t] anti-inflammatory[1r,1u] and analgesic[1u] agents, and as precursors for the synthesis of antibiotics.[1v–x] The polymers based on norbornene derivatives were shown to exhibit good antimicrobial activity.[2] Another important area of applications of norbornene derivatives is the agricultural industry—including insecticides,[3a] fungicides,[3b] herbicides and antibacterial agents.[3]

Due to the pharmacological properties of the bicyclic skeleton, the epoxynorbornanes (**1**) are of interest as potential biologically active systems or as intermediates for the synthesis of new classes of heterocyclic compounds. Cyclization reactions of epoxides are very interesting and important, because they form rearranged products with different properties. Epoxyimides of norbornanes can also participate in such reactions. The reactions of intramolecular cyclization of epoxides are widely used for the design of various oxygen, nitrogen and sulfur containing heterocyclic systems.[4]

The high stability of *exo*-epoxynorbornane (**1**) and its derivatives in the reactions of intermolecular epoxide opening has been demonstrated in a number of studies.[5] This stability is caused by significant steric hindrance of the *endo*-region of the skeleton for the nucleophilic attack. However, epoxynorbornanes which contain nucleophilic groups in the *endo*-region of the carbon bicycle [**2**, X = C(O)NR_2, C(O)OR, CH_2NHSO_2Alk(Ar), $CH_2NHC(O)NHAr$, CH_2NHCH_2Alk(Ar)], can easily undergo intramolecular heterocyclization reactions. The formation of different oxygen- (**3**) and nitrogen-containing (**4**) tricyclic systems has been described in our previous works.[6]

In the present study, we focus on the reactivity of epoxyimide derivatives (**5**) and their products. The epoxyimide derivatives of norbornane have been scarcely represented in literature and there have not been many attempts to reveal the reactivity of this

[a]*Department of Organic Chemistry, Dnepropetrovsk National University, Dnepropetrovsk 49010, Ukraine*
[b]*Department of Chemistry and Biochemistry, Interdisciplinary Center for Nanotoxicity, Jackson State University, 1400 J.R. Lynch Street, P.O. Box 17910, Jackson, MS 39217-0510, USA. E-mail: jerzy@icnanotox.org; Fax: +1(601)979-7823*
[c]*Institute of Molecular Biology and Genetics, Department of Molecular Biophysics, National Academy of Sciences, 150 Zabolotnoho, Kiev 03143, Ukraine*
[d]*STC "Institute for Single Crystals", National Academy of Sciences of Ukraine, 60 Lenina ave., Kharkiv 61001, Ukraine*

† Electronic supplementary information (ESI) available: ^{1}H NMR spectra of compounds **9–12**, and mass spectra and the molecular structures of **10a**, **11e** and **12k**. CCDC reference numbers 706778–706780. For ESI and crystallographic data in CIF or other electronic format see DOI: 10.1039/b917850c

 This journal is © The Royal Society of Chemistry 2010

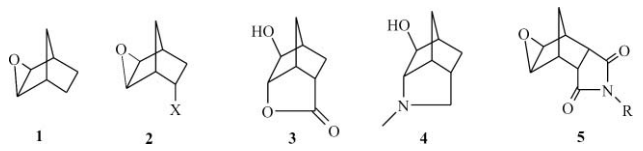

class of the nitrogen-containing polycyclic compounds. On one hand, due to the capability to further transform reaction centers, namely, the epoxide ring and imide fragment, these compounds can be examined as prospective candidates for transformation into different heteropolycyclic systems. It is mostly because of the presence of the epoxide ring and imide fragment in favorable orientation to each other. However, the high stability of the epoxide ring is the principle feature of the reactions for the epoxyimide derivatives of norbornane in neutral, alkaline and in some cases also in acidic solutions.[7] Increased stability of this type compound, related to the molecular rearrangement in an acidic solution, is induced by the low stability of carbcations containing electron-withdrawing groups.[8] According to the results of our previous work, the norbornane epoxyimides can react only with active enough reagents, for example, lithium aluminium hydride.[9] The heterocyclic systems (**7**, **8**) have been obtained by reduction of epoxyimide (**6**) in various proportions, depending on the reaction conditions.

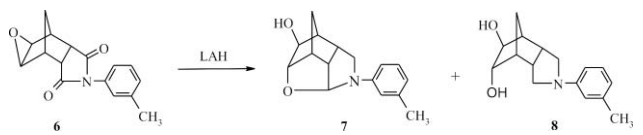

The purpose of this work was the development of new approaches for the transformation of the epoxyimides of norbornane into new heterocyclic compounds, particularly, investigation of the reactivity of these compounds in the presence of sodium ethoxide. The basic idea of the research was to use the stronger base in comparison with lithium aluminium hydride to generate one of two types of possible intermediates (**A** or **B**), which results in the formation of one of two heterocyclic systems (**C**, **D**) through the intramolecular cyclization.

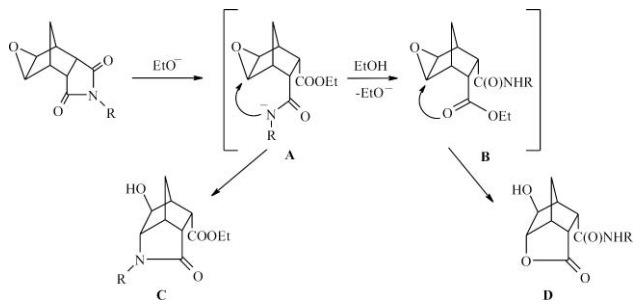

Results and discussion

1. Synthesis and products identification

A number of known (**9a**, **b**, **d**, **e**, **h–j**, **l**)[10] and new epoxides (**9c**, **f**, **g**, **k**, **m–p**) was selected for investigation. These compounds were synthesized by oxidation of the corresponding imides using performic acid *in situ* according to the classic procedure.[1q,10]

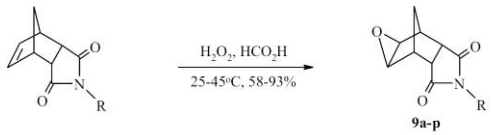

R = CH_3 (**a**), C_3H_7 (**b**), i-C_3H_7 (**c**), CH_2Ph (**d**), $C_6H_4CH_3$-p (**e**), $C_6H_3(CH_3)_2$-2,6 (**f**), $C_6H_3(CH_3)_2$-2,5 (**g**), $C_6H_4OCH_3$-p (**h**), C_6H_4Br-p (**i**), C_6H_5 (**j**), $C_6H_4NO_2$-m (**k**), $C_6H_4NO_2$-p (**l**), $C_6H_4CO_2Et$-p (**m**), 2-thiadiazolyl (**n**), C_6H_{11}-cyclo (**o**), 6-quinolyl (**p**)

Sodium ethoxide was chosen as a reagent and used as a 1 M solution in pure ethanol. It has been proved that the substrate was fully converted into products of the reaction by the action of one equivalent of reagent. It is also necessary to state that the type of products formed was governed mainly by the character of the substituent at the nitrogen atom of the epoxyimide. Three groups of the compounds were selected according to spectral analysis of the transformation products. The ethanolysis reaction of epoxyimides containing an alkyl and benzyl substituent at the nitrogen atom results in the formation of the corresponding dihydroxyimides (**10a–d**).

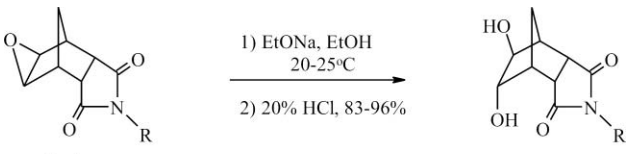

R = CH_3 (**a**), C_3H_7 (**b**), i-C_3H_7 (**c**), CH_2Ph (**d**)

The nature of the products of ethanolysis for the epoxyimides containing aryl substituents strongly depends on the electronic nature of this substituent. The reactions of epoxides (**9e–i**), containing electron-donor substituents, result in the formation of *endo*-9-carbamoyl-*exo*-2-hydroxy-5-oxo-4-oxatricyclo[4.2.1.$0^{3,7}$]nonanes (**11e–i**), while in the case of the absence of an electron-donor group or the presence of an electron-withdrawing group in the epoxyimide, the *exo*-2-hydroxy-5-oxo-4-azatricyclo[4.2.1.$0^{3,7}$]nonan-*endo*-9-carboxylic acids (**12j–n**) were obtained as unique product isomers of the ethanolysis reaction. Under similar conditions, epoxides (**9o**, **p**) form the mixtures of compounds (**10e**, **11j**) and (**11k**, **12o**). These compounds were obtained by fractional crystallization using 2-propanol.

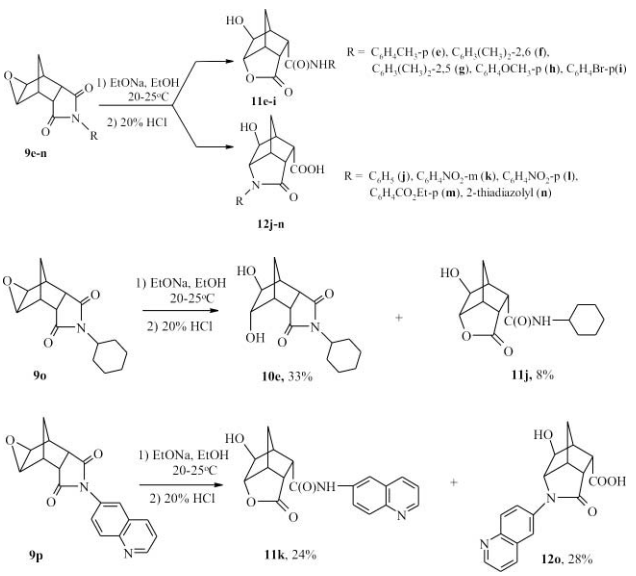

The analysis of the IR spectra of synthesized products leads to following conclusions: the spectra of all products are characterized by the absence of absorption bands in the region of 860–850 cm^{-1}, which corresponds to the stretching vibrations of the C–O bond in the epoxide cycle. Also, the presence of intense absorption bands in the region of 3500–3300 cm^{-1} (ν OH) has been detected. Additionally, it is necessary to state the presence of absorption bands of the carbonyl groups of the imide cycle in the diol molecules (**10**) in the 1780–1750 and 1710–1680 cm^{-1} regions, and the presence of characteristic amide or lactam bands in the 1680–1650 cm^{-1} region in the spectra of compounds **11** and **12**.

The conclusions about the structures of three types of the synthesized systems have been revealed based on the analysis of ^{1}H NMR spectra. The position of the signals, *i.e.*, two doublets (5.10–4.87 ppm), characterizing the resonance of the *trans*-oriented hydroxy groups, is the principle feature of the dihydroxyimide (**10**) spectrum. The resonance of the H^2 and H^3 nuclei, which is specific for this type of *trans*-disubstituted compound,[11] is mostly characterized by two signals, *i.e*, the singlet of the H^2 proton (3.21–3.14 ppm) and the doublet of the H^3 proton (3.77–3.71 ppm). The signals of the H^2 and H^3 protons appear in the same order in the ^{1}H NMR spectra of amidolactones (**11**),[12] while the H^2 proton is characterized by the weaker field signal (singlet) in the spectrum of azabrendanons (**12**). In addition, the spectra of lactones (**11**) are characterized by the presence of the signal of the amide proton in the field of 11.22–9.37 ppm, and ^{1}H NMR spectra of azabrendanons (**12**) contain characteristic signals of the carboxyl group proton in the field of 12.73–12.26 ppm. The structures of three types of compounds (**10a**, **11e**, **12k**) were confirmed by X-ray diffraction analysis.

According to the X-ray diffraction data, both cyclopentane rings within the framework of compound **10a** (Fig. 1) adopt an envelope conformation. The deviation of the C7 atom from the mean plane of the remaining atoms of the C3···C4···C5···C6···C7 and the C6···C8···C2···C3···C7 rings is 0.88 and –0.89 Å, respectively. The tetrahydropyrrole ring has a very flattened envelope conformation. The deviation of the C8 atom from the mean plane of the other atoms of the ring is 0.10 Å.

The bicycloheptane fragment and the tetrahydropyrrole ring are fused in the *cis*-type of conformation (the H2-C2-C8-H8 torsion angle is 9°). The hydroxyl group at the C4 atom has *endo*- and the hydroxyl group at the C5 atom has *exo*-orientation (the C2-C3-C4-O3 and O4-C5-C6-C8 torsion angles are 51.8(1)° and –176.23(9)°, respectively). Such orientation of the hydroxyl groups leads to the appearance of the strong enough repulsion with the atoms of the five-membered heterocycle which manifested itself in the H5···C9 2.59 Å and O3···C1 2.60 Å shortened intramolecular contacts (the van der Waals radii sums[13] are 2.87 and 3.00 Å, respectively).

In the crystal phase, the molecule **10a** forms the two-dimensional network in the (1 0 –2) crystallographic plane due to the O4–H4O···O2′ (1–x, 1–y, 1–z) (H···O′ 2.03(2) Å O–H···O′ 167(2)°) and the O3–H3O···O1′ (–x, 0.5+y, 0.5–z) (H···O′ 2.00(2) Å O–H···O′ 164(2)°) intermolecular hydrogen bonds.

The compound **11e** exists in the crystal phase as a monosolvate with isopropanol (Fig. 2). The heterocycle adopts an envelope conformation. The deviation of the C6 atom from the mean plane of the remaining atoms of the ring is 0.64 Å. The bicycloheptane fragment has almost the same geometry as in structure **10a**. The deviation of the C7 atom from the mean plane of the remaining atoms of the two cyclopentane rings is –0.83 and –0.84 Å, respectively. The hydroxyl group at the C2 atom has *exo*-orientation (the O3-C2-C3-C4 torsion angle is –178.5(2)°). The substituent at the C4 atom has *endo*-orientation (the C2-C3-C4-C9 torsion angle is 65.1(2)°), and it is almost orthogonal with respect to the C3-C4 bond (the C3-C4-C9-O4 torsion angle is –86.2(3)°). Such conformation of this substituent causes the appearance of the H2···C9 and H4···H1N shortened intramolecular contacts (2.73 and 2.16 Å, as compared with the van der Waals radii sums 2.87 and 2.34 Å, respectively). The aromatic ring is not coplanar with the carbamide fragment (the C9-N1-C10-C15 torsion angle

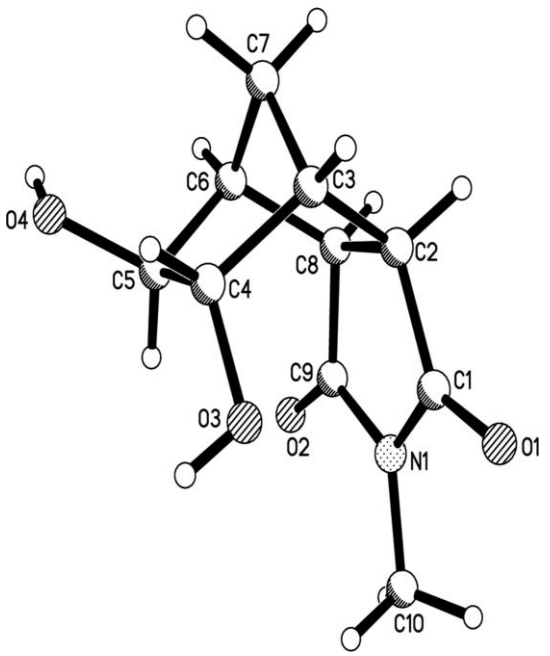

Fig. 1 The molecular structure of the compound **10a** with numeration of the non-hydrogen atoms used in the structural investigation.

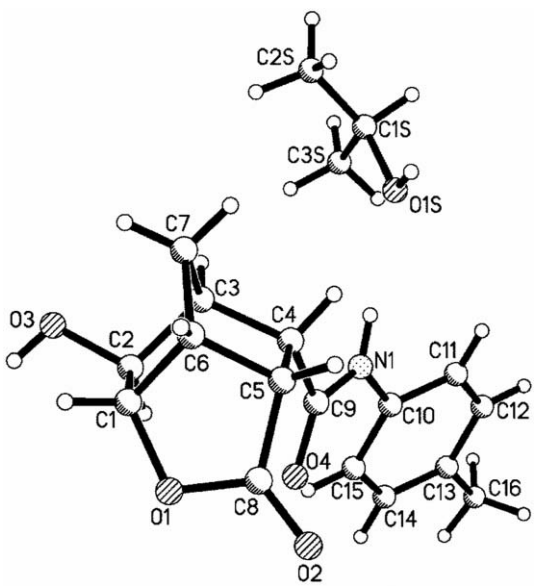

Fig. 2 The molecular structure of the compound **11e** with numeration of the non-hydrogen atoms used in the structural investigation.

 This journal is © The Royal Society of Chemistry 2010

is 30.1(3)°) due to the repulsion between the hydrogen atom of the phenyl substituent and the carbonyl group (the intramolecular shortened contacts are H15 · · · O4 2.42 Å (2.46 Å) and H15 · · · C9 2.83 Å (2.87 Å)).

In the crystal, the molecules **11e** form the two-dimensional network in the (0 0 1) crystallographic plane due to the formation of the O3–H3O · · · O2′ (1–x, –0.5+y, 1.5–z) (H · · · O 1.89 Å, O–H · · · O 172°), N1–H1N · · · O1S (0.5–x, 0.5+y, z) (H · · · O 2.09 Å N–H · · · O 176°) and O1S–H1Sa · · · O3′ (0.5–x, 0.5+y, z) (H · · · O 1.97 Å O–H · · · O 167°) intermolecular hydrogen bonds. The formation of the hydrogen bonds also causes, probably, some elongation of the N1–C9 (1.352(3) Å) and N1–C10 (1.422(3) Å) bond as compared with their mean values of 1.334 and 1.380 Å,[14] and the shortening of the O1S–C1S (1.394(2) Å) bond (mean value is 1.432 Å).

The conformation of the framework in the compound **12k** is very similar to the one in **11e** (Fig. 3). All five-membered rings adopt an envelope conformation. The deviation of the C6 atom from the mean plane of the remaining atoms of the tetrahydropyrrole ring and deviation of the C7 atom from the mean planes of the two cyclopentane rings are –0.60, 0.84 and –0.85 Å, respectively.

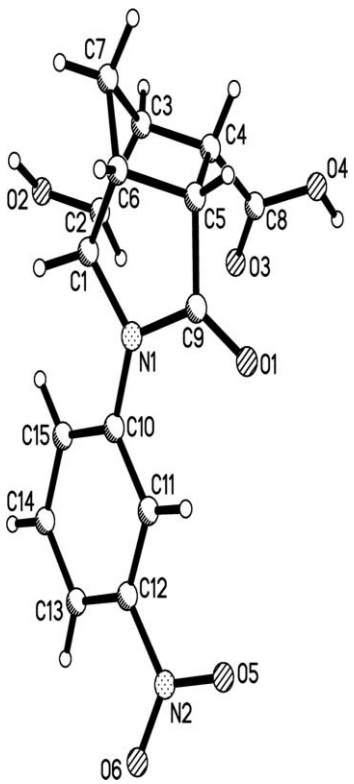

Fig. 3 The molecular structure of the compound **12k** with numeration of the non-hydrogen atoms used in the structural investigation.

Similar to structures **10a** and **11e**, the hydroxyl group at the C2 atom has *exo*-orientation (the O2-C2-C3-C4 torsion angle is –174.8(1)°). The carboxyl group adopts *endo*-orientation and it is twisted relative to the C3–C4 bond (the C2-C3-C4-C8 and C3-C4-C8-O3 torsion angles are 64.5(1)° and –31.7(2)°, respectively). The aromatic ring of the substituent at the N1 atom is twisted relative to the plane of the heterocycle (the C9-N1-C10-C11 torsion angle is 28.9(2)°). This is caused by the repulsion between the atoms of the benzene ring and framework (the shortened intramolecular contacts: H1 · · · C15 2.75 Å (2.87 Å), H1 · · · H15 2.27 Å (2.34 Å), H11 · · · O1 2.32 Å (2.46 Å), H15 · · · C1 2.53 Å (2.87 Å), H15 · · · C2 2.73 Å (2.87 Å)). The nitro group is non-coplanar to the plane of the aromatic ring (the O2-N2-C12-C11 torsion angle is –20.0(2)°).

The crystal **12k** forms the two-dimensional network in the (0 1 1) crystallographic plane due to the O4–H4O · · · O3′ (–x, 1–y, –z) (H · · · O 1.79(2) Å O–H · · · O 173(2)°) and O2–H2O · · · O1′ (1+x, y, z) (H · · · O 1.99(2) Å O–H · · · O 171(2)°) intermolecular hydrogen bonds. Formation of the O2–H2O · · · O1 hydrogen bond results also in the appearance of the H7a · · · H2O (2.22 Å) intramolecular shortened contact (sum of the van der Waals radii is 2.34 Å) due to the orientation of the hydrogen atom of the hydroxyl group toward the oxygen atom.

To rationalize the observed reactivity pattern and to better understand the mechanisms of the competitive cyclizations promoted by the ethoxy anion of sodium ethoxide, it is useful to perform a theoretical study of the reactions of substituted epoxyimides. According to the experimental results, three different classes of compound were generated during the ethanolysis reaction depending on the nature of the substituent. The most interesting representatives of the alkyl, electron-donor aryl and electron-withdrawing aryl epoxyimides were selected for the computational investigation: **9a**, **9e** and **9l**, respectively. Our main goal is to address the following issues: (1) Why do the reactions of alkyl-substituted epoxyimides lead to dihydroxyimides? (2) How does the character of the aryl substituent influence the nature of reaction products formed?

2. Computational study

In order to ascertain the mechanism of formation of the newly synthesized heterocyclic systems we have carried out a detailed computational investigation of the potential energy surfaces for the ethanolysis reaction of norbornane epoxyimides (**9a**,**e**,**l**) containing substituents of different character. Since the process takes place in polar protic media (ethanol), the careful study of the mechanism should also include the solvent effects, which could be taken into account using the self-consistent reaction field (SCRF) method or supermolecular approach. Firstly, let us briefly summarize the results of recently performed investigations for related systems.

There have been a number of computational studies on related systems. The base-catalyzed and general base/acid catalyzed methanolysis of formamide was analyzed by Štrajbl *et al.* at the DFT level of theory as a reference solution reaction for studies of serine proteases. According to their results, the methanolysis of formamide with water as the general base is a concerted process. However, the reaction with histidine as the general base involves a stepwise mechanism with a shallow surface that can allow for some population of both the stepwise and concerted pathways. The authors also provided a reliable estimate for the acidity constant of the amide nitrogen in the tetrahedral intermediate.[15] In addition, the alcoholysis reaction was studied for 1,2-thiazetidine-1,1-dioxide and its *N*-methyl derivative by He *et al.*[16] The PCM approach was applied in order to estimate the influence of methanol as a polar solvent (for the uncatalyzed reaction, ref. 16*a*). All possible reaction pathways were discussed and compared. The

authors found that bulk solvent effects have little effect on the alcoholysis mechanism.[16a] It was noticed that water- and alcohol-assisted alcoholysis mechanisms are similar to the non-water ones. However, catalytic water/alcohol molecules reduce the activation energy greatly compared with the uncatalyzed reaction.[16b]

The similar reaction mechanisms were also studied theoretically for the amide and ester hydrolysis. Zhan *et al.* investigated the reaction pathways and solvent effects for the base-catalyzed hydrolysis of alkyl esters in aqueous solution using a hybrid supermolecule-polarizable continuum approach. It is interesting to note that, according to their results, the extremely large solvent shifts of the energy barriers for the first step of the hydrolysis of the methyl esters are attributed mainly to the contributions of the bulk solvent effects. The explicitly included water molecules play a significant role only by assisting the proton transfer in the second step of the reaction.[17]

A hybrid supermolecule-polarizable continuum approach was also applied for the investigation of alkaline hydrolysis of a series of amides by Xiong *et al.*[18a] The calculated results reveal that the favorable transition state structure optimized for the tetrahedral intermediate formation for formamide may have three solvating water molecules remaining on the attacking hydroxide anion, and two additional water molecules attached to the carbonyl oxygen of formamide. Interestingly, the total number of water molecules hydrogen-bonded with the attacking hydroxide in the transition state decreases from three for formamide to two for *N*-substituted derivatives (*N*-methylacetamide, *N*,*N*-dimethylformamide and *N*,*N*-dimethylacetamide). Thus, the larger substituents of the amide hinder the solvent water molecules approaching the attacking hydroxide oxygen in the transition state. Cheshmedzhieva *et al.* performed a comparative computational and experimental study of the alkaline hydrolysis of secondary amides.[19] Their conclusions were analogous to the ones derived by Zhan *et al*.[17] The auxiliary water molecule does not play a substantial catalytic role during the first stage of the hydrolysis process. During the second step, the C–N breaking process, the proton transfer from the water molecule is essential for the stabilization of the $AlkNH^-$ anion when the leaving group is an aliphatic amine. In the case of acetanilide, the proton transfer toward the leaving group, which stabilizes the anion, appears to be less important because of the higher stability of the $PhNH^-$ anion.[19]

Among various quantum-chemical approaches, the methods based on the density functional theory offer the best choice to obtain results for large systems in reasonable time and acceptable accuracy. It is well known that the B3LYP functional could provide an adequate description of relatively strong covalent-[15,16a,20] and hydrogen-bonded[21] interactions that are important in the ethanolysis reaction. A number of published studies devoted to nucleophilic substitution reactions have shown a good performance in the proper description of hydrolysis and alcoholysis reaction mechanisms[15,16a,20a] of this level of theory.

In the present work, we performed the full geometry optimization for all reactive species at the DFT level of theory, using the polarizable continuum method (PCM) for the estimation of the bulk solvent effect as a highly promising compromise between reliable system description and acceptable computational efforts. It is also necessary to state that most published works employed PCM or other SCRF methods to estimate the influence of polar solvents on the energies of only the gas phase optimized structures.[16a,18a,19] Unlike water, whose bulk properties are entirely governed by hydrogen bonding, ethanol has both hydrogen bonding and hydrophobic interactions. In the PCM approach, the solute molecule is embedded in a cavity in a dielectric medium that represents the solvent. Solute–solvent interactions are described by a reaction potential arising from the presence of the dielectric medium, which is sufficient for description of the solvent properties in the studied systems. Considering the bulk of the ethyl group of ethanol molecules and the complexity of the bicyclic epoxyimide system, we assumed that the addition of explicit solvent molecules to the reaction mixture would not significantly impact the possible mechanisms of ethanolysis reaction, except of potential proton transfer processes. The studies discussed earlier performed by Zhan *et al.*[17] and Cheshmedzhieva *et al.*[19] also support the adequacy of our approach.

Due to significant steric hindrance of the *endo*-region of the imide's skeleton, the intermolecular opening of the epoxide cycle is impossible under the optimized conditions,[22] so the only possible pathway for the first stage of the transformation is attack of the ethoxy anion on the carbon atoms of the imide ring from the *exo*-region of the molecule.

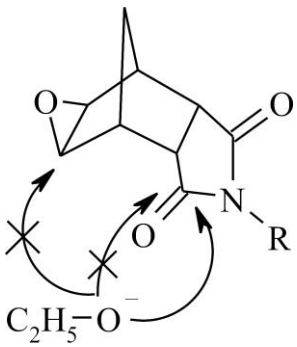

At first, we consider the ethanolysis reaction of the norbornane epoxyimide containing alkyl substituents at the nitrogen atom. The reaction starts from the addition of the ethoxy anion to the carbonyl carbon atom. Thus, the ethanolysis of norbornane epoxyimide (**9a**) containing methyl substituents at the nitrogen atom of the imide cycle involves the formation of a tetrahedral intermediate (**INT1a**) *via* transition state (**TS1a**). The normal mode vector of imaginary frequency for **TS1a** depicts the motion of the oxygen atom from the ethoxy anion toward the carbonyl carbon (see ESI†). In the transition state, the formed C–O bond distance equals 2.245 Å. Note that the CN bond tends to become longer in the course of the nucleophilic attack. In the initial imides, both CO and CN bonds have partial double bond character. However, when the nucleophilic attack is completed, the imide oxygen is negatively charged and the resonance is lost, which causes the CN bond to become a single bond. The corresponding lengthening of the CN bond occurs gradually as the tetrahedral intermediate **INT1a** is being formed.

Based on the analysis of the potential energy surface, two competing reaction pathways were found for the intermediate (**INT1a**) transformation. These pathways share a common first step. Pathway 1 corresponds to breaking of the C–N bond of the imide cycle and proceeds *via* transition state (**TS2a**), and results in formation of the anion of epoxyamidoacid ester (**INT2a**). Pathway 2 represents the alternative mechanism where the oxygen atom of

 This journal is © The Royal Society of Chemistry 2010

the carbonyl group interacts with the carbon atom of the epoxide cycle without cleavage of the imide cycle. The normal mode vector of imaginary frequency of the transition state **TS3a** indicates the breaking of the O–C σ-bond of the epoxide cycle and the formation of the C–O σ-bond of cyclic acetal (see ESI†). Optimization of the transition state (**TS3a**), following the transition vector leads to the formation of the anionic heterocyclic intermediate (**INT3a**).

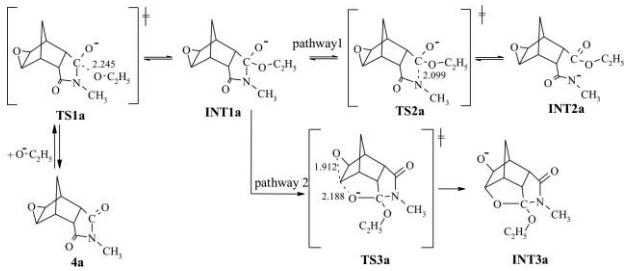

The calculated values of potential energy (Δ*E*), enthalpy (Δ*H*), and Gibbs free energy (Δ*G*) relative to the separate reactants for all fully optimized critical structures are given in Table 1. The energetic diagrams for the change of relative potential energy and free Gibbs energy during the possible pathways for the ethanolysis reaction of the epoxyimide (**9a**) are shown in Fig. 4. As one can see from Fig. 4, the change of the description for the energy diagram from the total energy in solution to free Gibbs energy terms affects only the first stage of the ethanolysis reaction. The values of the activation barrier parameters are not altered for the **INT1a** transformation pathways. There are a couple of possible reasons for the increase in the reaction barrier for the process of addition of the ethoxy anion to the epoxyimide compound. At first, the better solvation of the separate ethoxy anion and epoxyimide relative to that of transition states and intermediates where the negative charge is delocalized over the entire molecule is the origin of the enhanced barrier. This result is similar to what has been found in other ion–molecule reactions.[23] Secondly, the free energy corrections based on the harmonic vibrational analysis could produce an error in the calculation of the absolute entropy for each molecular species that gives rise to Gibbs free energy change. It was underlined by Zhan *et al.* for the alkaline hydrolysis[18] that the harmonic approximation is inadequate, particularly for the normal vibration modes with low frequencies. In other words, the values of the relative Gibbs free energies significantly differ compared to the corresponding relative enthalpy data during intermolecular interactions (4a + $C_2H_5O^-$) because of the replacement of three from a total of six translational degrees of freedom by rotational and vibrational ones.[24] We suppose that the impact of these errors on the general description of the activation free energy diagram for the studied reaction would be smaller if compared to the hydrolysis process, but nevertheless, they would cause some underestimation of the stability of product formed.

Table 1 Energies, Δ*E* (in kcal mol^{-1}), enthalpies, Δ*H* (at 1 atm, 298.15 K, in kcal mol^{-1}), and Gibbs free energies, Δ*G* (at 1 atm, 298.15 K, in kcal mol^{-1}) of transition states and intermediates relative to the separate reactants along the possible pathways for the ethanolysis of the epoxyimide (**9a**) at the PCM/B3LYP/6-31+G(d) level of theory

	Δ*E*	Δ*H*	Δ*G*
React (**9a** + $C_2H_5O^-$)	0.00	0.00	0.00
TS1a	5.34	6.42	14.99
INT1a	–0.40	1.23	10.37
TS2a	5.54	6.59	15.50
INT2a	2.75	3.45	10.88
TS3a	16.77	20.43	28.52
INT3a	–13.95	–10.25	–2.04

The first stage of the reaction proceeds through **TS1a** with activation free Gibbs energy of 14.99 kcal mol^{-1} (Fig. 4). Thermodynamic and kinetic analyses can further illustrate the possibility of a reaction in both directions. As can be seen from the energy diagram (Fig. 4), pathway 1, which includes the breaking of the C–N bond, is characterized by a lower activation barrier for the second stage of the reaction ($\Delta G^{\ddagger}$ = 5.13 kcal mol^{-1}) if compared to pathway 2 (without breaking of the imide cycle) where the activation Gibbs free energy barrier equals 17.65 kcal mol^{-1}. However, based on the low activation barrier for the transformation of **INT2a** back to **INT1a** (4.62 kcal mol^{-1}), one may conclude that this stage is reversible and, due to its endothermic character, equilibrium shifts to **INT1a**. In contrast, pathway 2 results in the formation of the stable intermediate (**INT3a**). The

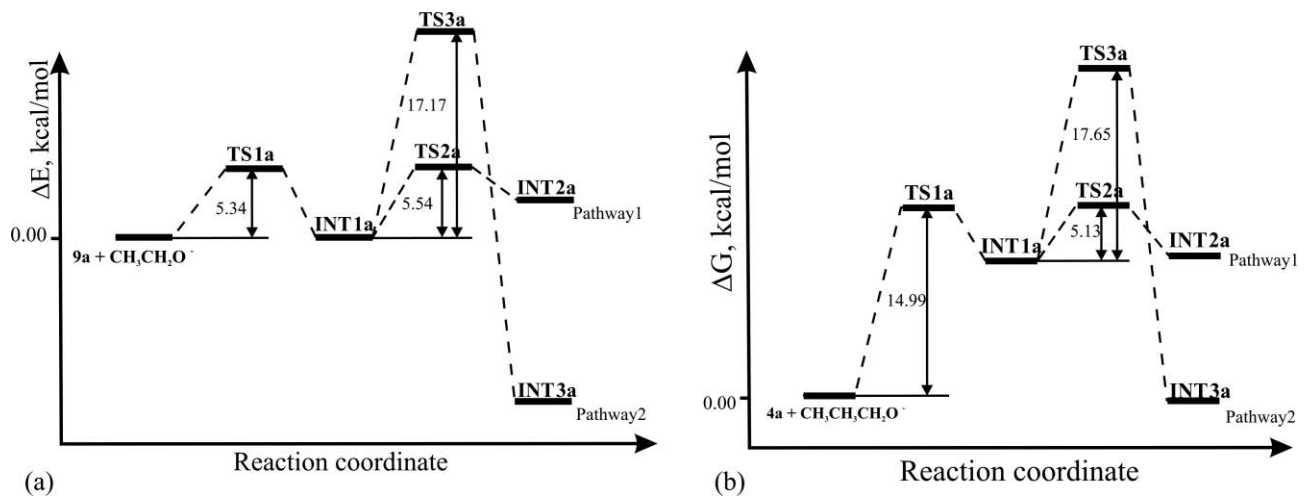

Fig. 4 Potential energy (a) and free Gibbs energy (b) diagrams along the possible pathways for the ethanolysis of epoxyimide (**9a**) (PCM/B3LYP/6-31+G(d) level of theory).

Table 2 Values of equilibrium (K) and rate constants for forward (k_f, s^{-1}) and reverse (k_r, s^{-1}) reactions

	K	k_f/s^{-1}	k_r/s^{-1}
INT1a → INT2a	4.23×10^{-1}	1.08×10^{9}	2.55×10^{9}
INT1a → INT3a	2.90×10^{9}	7.17×10^{-1}	2.47×10^{-10}

high barrier of the reverse reaction ($\Delta G^{\ddagger} = 30.56$ kcal mol^{-1}, see Fig. 4) provides evidence for the kinetic stability of **INT3a** and for the removal of the tetrahedral intermediate from the equilibrium. These statements are also supported by the results of kinetic simulation of the reaction pathways.

The equilibrium and rate constants of the considered forward and reverse reactions (see Calculations section for details) are collected in Table 2. Predicted kinetic curves are displayed in Fig. 5. The equilibration process can be divided into two steps. During the first step (Fig. 5a) which lasts for virtually an instant (within *ca.* 2×10^{-9} s) the kinetically favorable reaction **INT1a** → **INT2a** leads to formation of the intermediate **INT2a**. In this step, the stationary relative concentrations of **INT1a** (70%) and **INT2a** (30%) are reached while concentration of **INT3a** is still negligibly small. In the second step (Fig. 5b) the thermodynamically favorable reaction **INT1a** → **INT3a** leads to the formation of **INT3a** product at the expense of **INT1a** and **INT2a**. The population of **INT2a** decreases following the scheme: **INT2a** → **INT1a** → **INT3a**. Finally, the concentrations of **INT1a** and **INT2a** decrease to zero while the concentration of **INT3a** reaches its equilibrium value of 100% within about 10 s. Thus, one may conclude that pathway 1, resulting in the formation of anion (**INT2a**), is strongly unfavorable for imides with donor alkyl substituents at the nitrogen atom. Instead of the formation of the endothermic intermediate (**INT2a**), the primary product of the ethoxy-anion addition (**INT1a**) undergoes intramolecular heterocyclization. This process results in formation of the cyclic acetal (**INT3a**), which governs further formation of products with the structure of dihydroxyimide (**10a**). It is illustrated by the following scheme:

Thus, the primary product of the ethoxy anion addition for the imides with donor alkyl substituents at the nitrogen atom (for

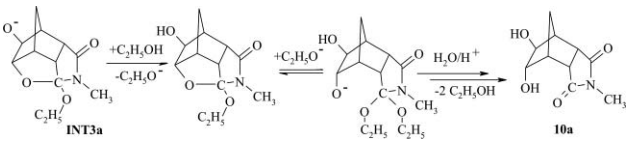

example **9a**) undergoes intramolecular heterocyclization without breaking of the imide cycle, with the subsequent formation of products with the structure of dihydroxyimide. This might be explained mainly by the instability of the intermediates formed due to the imide ring opening process.

The second part of the computational work focuses on the ethanolysis reaction of norbornane epoxyimide containing aromatic substituents at the nitrogen atom. The tolyl *N*-substituted derivative (**9e**) was chosen as a reference electron-donor aromatic compound and nitrobenzyl *N*-subtituted (**9l**) as an electron-withdrawing one. As in the case of ethanolysis of methyl norbornane epoxyimide, the reaction starts from the addition of the ethoxy anion to the carbonyl carbon atom with the subsequent process of breaking of the CN bond.

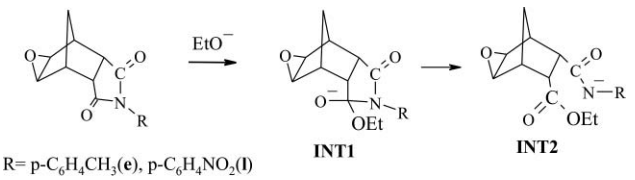

The results of our theoretical research reveal that, in contrast to the ethanolysis of the epoxyimide (**9a**), the interaction of the ethoxy anion with aryl epoxyimide derivatives (**9e**,**l**) proceeds through the formation of tetrahedral intermediate (**INT1**), which does not involve any activation barrier. In the next step, the transformation of epoxyimides (**9e**,**l**) involves a ring-opening process with breaking of the C–N bond. The potential energy surfaces for the studied ethanolysis reaction for **9e** seem to be very flat because all attempts we made to locate the PCM/B3LYP/6-31+G(d) transition structures failed, yielding either reactants or the intermediate products.

The calculated values of energy (ΔE), enthalpy (ΔH) and Gibbs free energy (ΔG) relative to the separate reactants for all fully

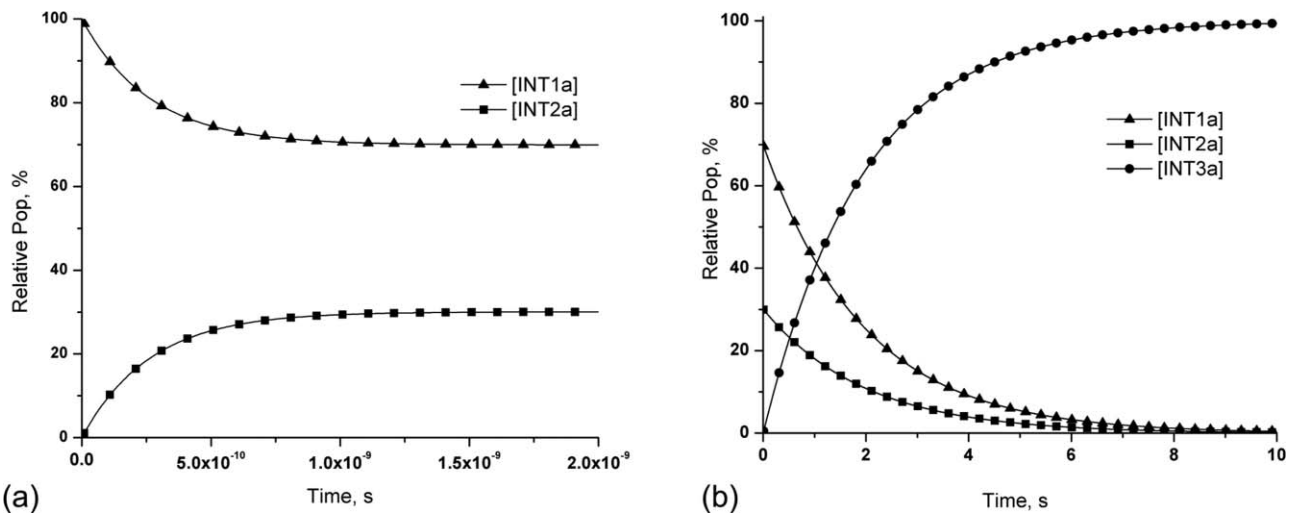

Fig. 5 Kinetics simulation of **INT1a** ⇌ **INT2a** and **INT1a** ⇌ **INT3a** transformation processes.

 This journal is © The Royal Society of Chemistry 2010

Table 3 Energies, ΔE (in kcal mol^{-1}), enthalpies, ΔH (at 1 atm, 298.15 K, in kcal mol^{-1}), and Gibbs free energies, ΔG (at 1 atm, 298.15 K, in kcal mol^{-1}) of intermediates relative to the separate reactants along the mechanistic pathway for the ethanolysis of the epoxyimides (**9e**, **9l**) at the PCM/B3LYP/6-31+G(d) level of theory

	$\Delta E^{\ddagger}$	$\Delta H^{\ddagger}$	$\Delta G^{\ddagger}$
React (**9e** + $C_2H_5O^-$)	0.00	0.00	0.00
INT1e	0.05	0.33	11.07
INT2e	−0.47	0.33	9.18
React (**9l** + $C_2H_5O^-$)	0.00	0.00	0.00
INT1l	−6.48	−5.99	4.14
INT2l	−18.13	−6.01	−9.78

optimized critical structures are given in Table 3. The energetic diagrams for the activation energy and free Gibbs energy changes of the possible pathways for the ethanolysis reaction of the epoxyimides (**9e**,**l**) are shown in Fig. 6 and 7, respectively. In terms of zero-point corrected energy values, the DFT calculations predict a slightly exothermic formation of the epoxyamido acid esters (**INT2**) in the case of norbornane epoxyimides with aryl substituents (**9e**,**l**). The initial formation of a tetrahedral intermediate and breaking of the imide cycle are the barrier-free processes for the epoxyimides (**9e**,**l**) and they proceed with a net energy gain of 0.47 kcal mol^{-1} for **9e** and 18.13 kcal mol^{-1} for **9l**. From the diagrams of free Gibbs energy, one can see the same reactant's energy shift as for the methyl-substituted epoxyimide's ethanolysis reaction discussed earlier. The same reasons cause the changes in the relative Gibbs free energy profile (Fig. 6 and 7). The solvation favors the separate reactants over the transition states and intermediates, so that the free Gibbs energy of reactants is decreased relative to the intermediate energy value. This change also affects only the first stage of the process. However, on the surface of Gibbs free energy, the structure of **INT1** looks like it is located in the area of the transition state. In terms of free Gibbs energy, one can conclude that the ethanolysis reaction for the nitrobenzyl *N*-subtituted epoxyimide (**9l**) is a slightly

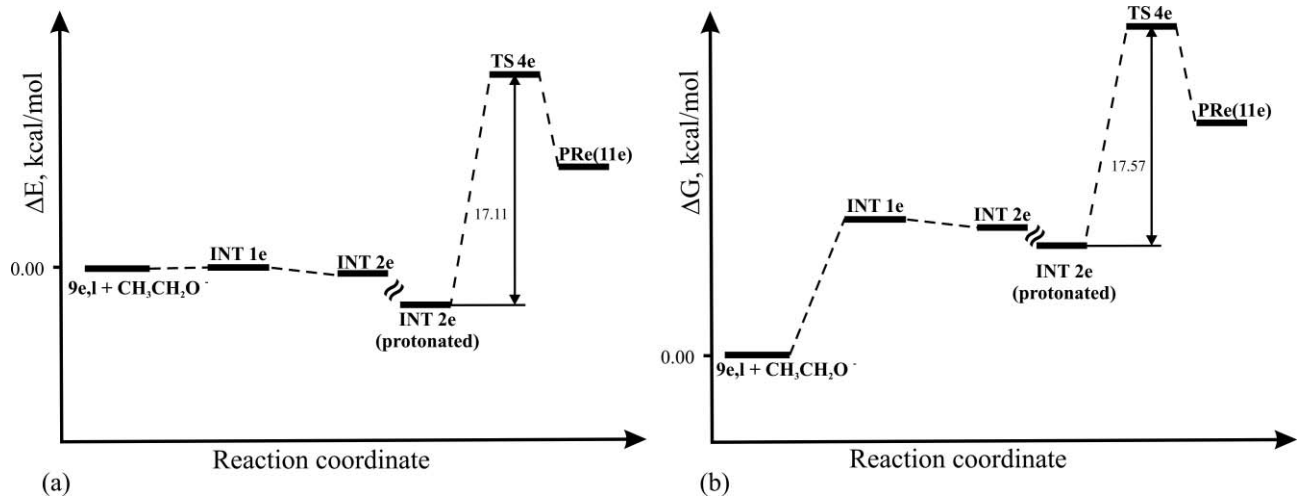

Fig. 6 Potential energy (a) and Gibbs free energy (b) diagrams for the ethanolysis reaction of the epoxyimide (**9e**) (PCM/B3LYP/6-31+G(d) level of theory).

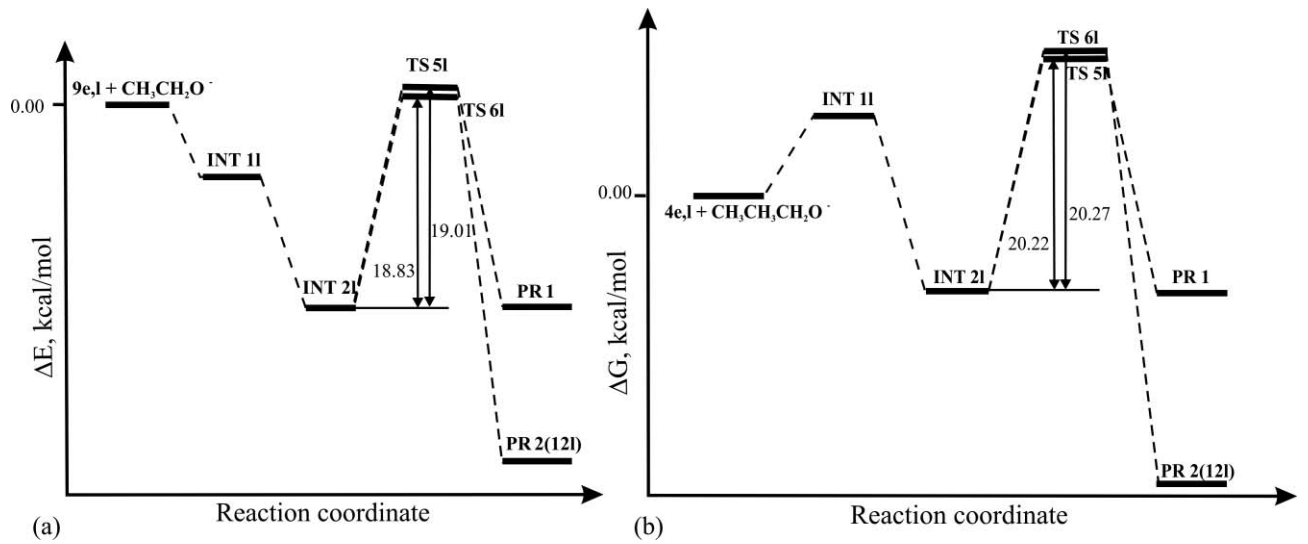

Fig. 7 Potential energy (a) and Gibbs free energy (b) diagrams for the ethanolysis reaction of the epoxyimide (**9l**) (PCM/B3LYP/6-31+G(d) level of theory).

exothermic process, while ethanolysis of tolyl *N*-substituted derivative (**9e**) leads to formation of the endothermic intermediate **INT2e**.

We assumed that stability of the formed intermediates, as well as the regiochemistry of further transformation of (**INT2e**,**l**), basically depends on the form adopted by the main fraction of (**INT2e**,**l**) in ethanol solution. In order to establish the significance of the acid–base equilibrium for the determination of further transformation of (**INT2e**,**l**), we evaluated the energy change corresponding to the proton transfer reactions from the ethanol molecule to the anion intermediate. Protonation can stabilize the formed intermediate and provide the possibility for further transformations. If the (**INT2e**,**l**) anion is a stronger base than the ethoxy anion, the intermediate adopts the neutral form and intramolecular cyclization with the ester group is more favorable. Otherwise, cyclization proceeds with a negatively charged deprotonated amide group.

A series of calculations were carried out based on the hybrid supermolecule-polarizable continuum approach, in which three solvent ethanol molecules were explicitly included in the supermolecular calculations. The bulk solvent effects were modeled as a polarzable dielectric continuum (PCM) surrounding the supermolecular reaction system.

As depicted in Scheme 1, three ethanol molecules were used for modeling the first solvation sphere for each of the reactants. Two solvent ethanol molecules simultaneously form strong hydrogen bonds with the amide nitrogen in (**INT2**) (N···H distances are equal to 1.880 and 1.924 Å for *p*-$C_6H_4CH_3$ derivative (**INT4e**) and to 1.921 and 1.986 Å for *p*-$C_6H_4NO_2$ derivative (**INT4l**)). The third ethanol molecule forms a hydrogen bond with the carbonyl oxygen of the amide (O···H distances are equal to 1.815 Å for **INT4e** and to 1.847 Å for **INT4l**). The hydroxyl group of the explicitly considered ethanol molecule can form three hydrogen bonds with the solvent molecules. Two of them correspond to the interaction of the hydroxyl oxygen with hydrogen atoms of solvent ethanol molecules (at O···H distances 1.862 and 1.867 Å). The third one is formed *via* interaction of hydroxyl hydrogen with the oxygen atom of the solvent (corresponding H···O distance is equal to 1.766 Å). The proton transfer proceeds from the solvated ethanol molecule $EtOH(EtOH)_3$ to the nitrogen atom of the amide to form the neutral species (Scheme 1). To keep the system equilibrium, the structure of the neutral form of the epoxyamido acid ester also includes three solvent molecules, while one of them was shifted to the second solvation shell (see Scheme 1). The values of the corresponding distances for C=O···H, N–H···O and O–H···H hydrogen bonds are 1.871, 1.905 and 1.804 Å for **INT5e** and 1.925, 1.867 and 1.791 Å for **INT5l**. The oxygen atom of the anionic form of ethanol can generate three hydrogen bonds to form the first solvation sphere (O···H distances are equal to 1.619, 1.617 and 1.635 Å).

Table 4 Activation energy, $\Delta E^{\ddagger}$ (in kcal mol^{-1}), enthalpy, $\Delta H^{\ddagger}$ (at 1 atm, 298.15 K, in kcal mol^{-1}), and Gibbs free energy, $\Delta G^{\ddagger}$ (at 1 atm, 298.15 K, in kcal mol^{-1}) barriers for the possible mechanisms of transformation for the aromatic intermediates (**INT2e**,**l**) at the PCM/B3LYP/6-31+G(d) level of theory

	$\Delta E^{\ddagger}$	$\Delta H^{\ddagger}$	$\Delta G^{\ddagger}$
INT2e(H) → TS4e	17.11	18.52	17.57
TS4e → Pre(11e)[a]	−7.25	−7.16	−6.61
INT2l → TS5l	19.01	19.42	20.22
TS5l → PR1l[a]	−20.72	−20.42	−20.85
INT2l → TS6l	18.83	19.37	20.27
TS6l → PR2(12l)[a]	−32.91	−33.81	−33.64

[a] Corresponding thermodynamic parameter barrier value for transition from the transition state to product

We evaluated the ΔG for the proton transfer reactions from the ethanol molecule to the anion intermediate for the substituted epoxyamido acid esters (**INT2e**,**l**) using the PCM/B3LYP/6-31+G(d) level of theory. Our calculations reveal that the anionic form is more favorable thermodynamically in the case of *p*-nitro aryl compound (**INT4l**) ($\Delta G = 5.37$ kcal mol^{-1}), while the *p*-tolyl derivative (**INT4e**) would favor the neutral state ($\Delta G = -3.79$ kcal mol^{-1}). This is in good agreement with the geometry features of the studied intermediates. The conjugation of the negative charge at the nitrogen atom with the aromatic ring increases in the case of electron-withdrawing substituents (**INT4l**). As a result, the anionic form of the intermediate becomes more favorable, while the formation of the neutral structure becomes preferable for electron-donor substituted compounds (**INT5e**).

In order to provide meaningful insight into the mechanisms for the ethanolysis reaction, the subsequent cyclization reactions were examined in detail. All possible ways of heterocyclization of the epoxyimides (**9e**,**l**) are shown in Scheme 2. The calculated values of activation energy ($\Delta E^{\ddagger}$), enthalpy ($\Delta H^{\ddagger}$) and Gibbs free energy ($\Delta G^{\ddagger}$) for all fully optimized structures for the possible pathways of heterocyclization are given in Table 4. The energetic diagrams for the activation energy and free Gibbs energy changes of the possible pathways for the heterocyclization reaction of the epoxyimides (**9e**,**l**) are shown in Fig. 6 and 7, respectively. The most plausible mechanism for the neutral *p*-tolyl derivative (**INT5e**) is based on the intramolecular lactonization reaction, where the breaking of the epoxide cycle is coupled with nucleophilic attack of the carbonyl oxygen atom of the ester group of the epoxyamido acid ester (**TS4e**). The activation free Gibbs energy barrier for this stage of the ethanolysis reaction is equal to 17.57 kcal mol^{-1}. The lengths of the corresponding formed and broken bonds are presented

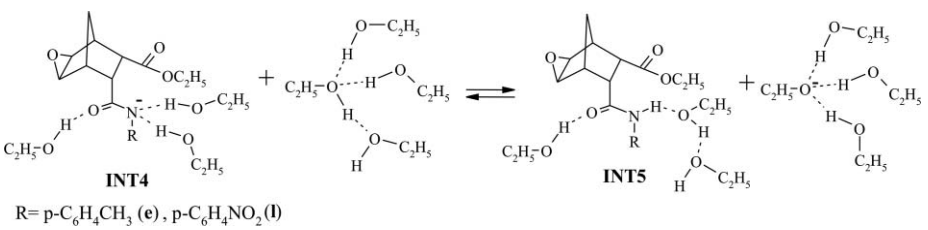

Scheme 1 Schematic representation of the proton transfer process from the ethanol molecule to the anion intermediate for the series of substituted epoxyamido acid esters.

 This journal is © The Royal Society of Chemistry 2010

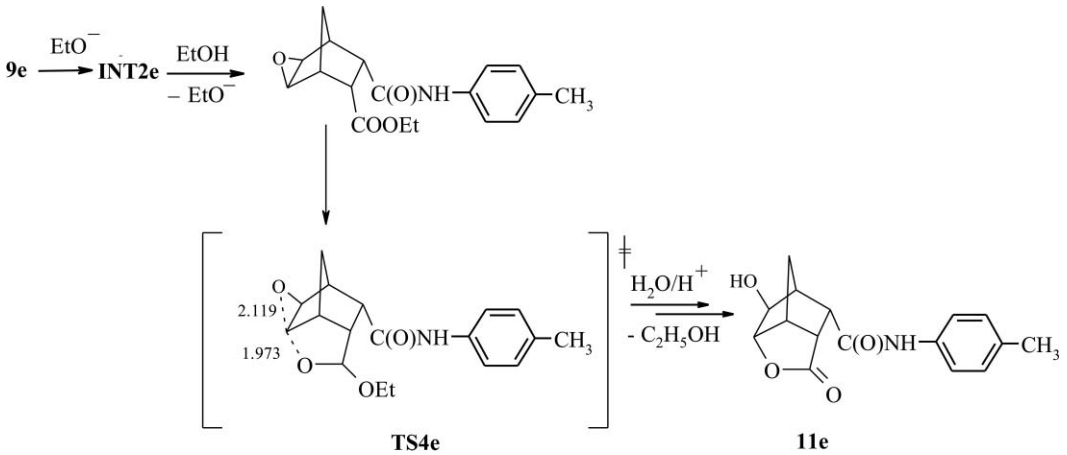

Scheme 2 Schematic representation of the possible cyclization mechanism for the intermediate of **9e** (PCM/B3LYP/6-31+G(d) level of theory).

in Scheme 2. The normal mode vector of imaginary frequency for **TS4e** clearly shows the simultaneous motions of the epoxide oxygen atom in the direction of the ring opening process and the ester oxygen atom to form the heterocyclic bond with the carbon atom of the norbornane derivative (see ESI†). As one can see from the diagram (Fig. 6), the reaction leads to the endothermic product formation. The product could be stabilized by surrounding solvent molecules, which form relatively strong hydrogen bonds with the negatively charged oxygen atom of the formed intermediate to prevent the reverse epoxide cycle formation.

We next studied cyclization steps for the *p*-nitro phenyl intermediate (**INT4l**, Scheme 3). The possible mechanism represents the opening of the epoxide cycle accompanied by the nucleophilic attack of the imide moiety, as depicted in Scheme 3. The transition states for O-attack and N-attack are computed as **TS5l** and **TS6l**, respectively. The lengths of the corresponding formed and broken bonds are presented in Scheme 3. **TS6l** is lower in energy than **TS5l** by 1.86 kcal mol^{-1}, while both processes result in the same Gibbs free energy change in the overall free energy diagram (Fig. 7). Thus, the preferred pathway is being determined by the stability of the product formed. As one can find from both of the diagrams, the formation of **PR1**, which corresponds to the O-attack process, is less favored compared to **PR2** formation. Produced during N-attack, the intermediate **PR2** is stabilized by 12.79 kcal mol^{-1} at the free Gibbs energy surface. This confirms the preference of the azabrendanon (**12l**) product formation. The results indicate the preference for N-attack that is consistent with the experimental study. According to our observations in the cyclization process, the lactamization (*via* N-attack) occurs rather than lactonization (*via* O-attack).

In summary, our results clearly show a trend of the substituent shift of the calculated free energy change for the ethanolysis of norbornane epoxyimides and indicate that the structural features of the starting epoxyimides determine the behavior of the cyclization pathways. We have revealed for the imides with donor alkyl substituents at the nitrogen atom (as in case **9a**) that the primary product of the ethoxy anion addition undergoes intramolecular heterocyclization without breaking of the imide cycle, with subsequent formation of products that possess the structure of dihydroxyimide. This might be explained mainly by

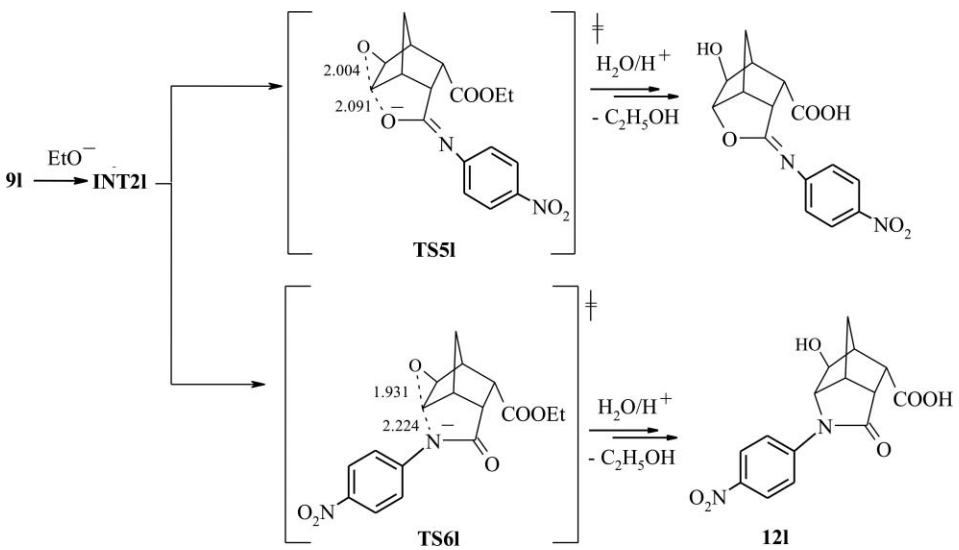

Scheme 3 Schematic representation of the possible cyclization mechanisms for the intermediate of **9l** (PCM/B3LYP/6-31+G(d) level of theory).

the instability of the intermediates formed due to the imide ring opening process. The mechanism of heterocyclization for aryl epoxyimide derivatives (**9e**,**l**) is determined by the position of acid–base equilibrium of the epoxyamido acid esters formed during the ethanolysis reaction. For this process, specific solvation of ethanolysis intermediates has the key influence on the formation of the azabrendanon or amidolactone products.

Conclusions

In this study we have carried out a systematic investigation of the ethanolysis reaction for the series of norbornane epoxyimides bearing alkyl and aryl substituents on the nitrogen atom. We established that interaction of the aryl-substituted epoxyimides of norbornane with sodium ethoxide yields heterocyclic compounds in preparatively useful yields and with complete regioselectivity. The reactions of epoxyimides containing aryl electron-donor substituents result in the formation of *endo*-9-carbamoyl-*exo*-2-hydroxy-5-oxo-4-oxatricyclo[4.2.1.$0^{3,7}$]nonanes, while in the case of the absence of an aryl electron-donor group (or presence of an aryl electron-withdrawing group) in the epoxyimide, *exo*-2-hydroxy-5-oxo-4-azatricyclo[4.2.1.$0^{3,7}$]nonan-*endo*-9-carboxylic acids were obtained as products of the ethanolysis reaction. Unexpectedly, the ethanolysis of alkyl-substituted epoxyimides led to dihydroxyimide formation as the major product. NMR study revealed the formation of several types of products of ethanolysis of various epoxyimides, the structures of representative compounds of the main classes were also determined using X-ray crystallography.

Theoretical calculations in combination with the experimental results offer a comprehensive understanding of the mechanism of the ethanolysis reaction. We found that substituents at the nitrogen atom of epoxyimides exerted remarkable effects on the regioselectivities in the ethanolysis reaction based on the solvent effects and intramolecular electronic interactions. Particularly, the preference for the formation of dihydroxyimides over heterocyclic systems for alkyl derivatives might be explained by the kinetic stability of the formed acetal intermediate over the competitive epoxyamido acid intermediate. The results of kinetic simulation suggest that the kinetically favorable reaction **INT1a** → **INT2a** leads to fast formation of intermediate **INT2a** (30%) within *ca.* 2×10^{-9} s. However, due to high thermodynamic stability of **INT3a** (equilibrium constant 2.90×10^{9}) the final mixture contains exclusively **INT3a**. The mechanism of heterocyclization for aryl epoxyimide derivatives is determined by the position of the acid–base equilibrium of epoxyamido acid intermediates formed during the reaction. This work represents a convenient and efficient approach for predicting the structures of formed heterocyclic systems under basic ethanol conditions depending on the substituent on the nitrogen atom of the norbornane epoxyimides.

Experimental section

General

All solvents for the reactions were dried and distilled immediately prior to use. Melting points were determined in capillary tubes and are uncorrected. Infrared spectra were recorded on a UR-20 or Paragon 500 FT-IR (Perkin Elmer) spectrometer using KBr pellets. ^{1}H NMR spectra were recorded at 200 and 300 MHz on a Varian spectrometer. Chemical shifts (δ) are reported in ppm relative to TMS in DMSO-d_6. EI mass spectra of compounds (**10a**, **11e**, **12k**) were recorded on an MX-1321 spectrometer (70 eV). For thin-layer chromatography (TLC) analysis, TLC plates (Silufol UV-254) were used with diethyl ether or 2-propanol as eluent and iodine vapor as developer. Elemental analyses were carried out on a Carlo Erba analyzer.

The synthesis of the unsaturated epoxyimides (**9a**, **b**, **d**, **e**, **h**, **i**, **j**, **k**, **p**) were performed by methods described in the literature[1q] and the yields were 76–98%.

General procedure for the synthesis of epoxyimides (9c, f, g, l, m, n, o)

A solution of 2.3 mL (0.04 mol) 50% hydrogen peroxide (aq) was added by drops under stirring to the corresponding bicyclo[2.2.1]hept-5-en-*endo*,*endo*-2,3-dicarboximide (0.02 mol) in 20–25 mL of 98% formic acid. The reaction mixture was stirred at the temperature 25 °C. The completion of reaction was monitored by TLC. The formed compound was dried in vacuum, and then 25–30 ml of ice-cold water was added. Product was filtered out, dried and purified by crystallization from 2-propanol.

***N*-Isopropyl-*exo*-5,6-epoxybicyclo[2.2.1]heptan-*endo*,*endo*-2,3-dicarboximide (9c).** White solid; mp 148-149 °C; 3.36 g (76.0%) yield. R_f 0.74 (2-propanol). Found: C, 65.09; H, 6.71; N, 6.39. $C_{12}H_{15}NO_3$ requires: C, 65.16; H, 6.79; N, 6.33%. IR (KBr, cm^{-1}): 3050, 1755, 1700, 1468, 1375, 1235, 1140, 860. ^{1}H NMR (200 MHz) δ_H 4.18 (1H, m, CH), 3.18 (1H, dd, *J* 3.1, 1.9 Hz, H^5), 3.16 (1H, dd, H^6), 3.08 (2H, m, $H^{2,3}$), 2.86 (2H, m, $H^{1,4}$), 1.34 (1H, d, *J* 10.0 Hz, H^{7s}), 1.25 (6H, d, $2CH_3$), 1.02 (1H, d, H^{7a}).

***N*-(*o*,*o*′-Dimethylphenyl)-*exo*-5,6-epoxybicyclo[2.2.1]heptan-*endo*,*endo*-2,3-dicarboximide (9f).** White solid; mp 212-214 °C; 5.34 g (94.4%) yield. R_f 0 (2-propanol). Found: C, 72.11; H, 6.09; N, 5.02. $C_{17}H_{17}NO_3$ requires: C, 72.08; H, 6.01; N, 4.95%. IR (KBr, cm^{-1}): 3045, 3012, 1780, 1720, 1522, 1390, 1190, 860. ^{1}H NMR (200 MHz) δ_H 7.30-7.14 (3H, m, H_{arom}), 3.60 (1H, dd, *J* 3.0, 1.8 Hz, H^5), 3.58 (1H, dd, H^6), 3.39 (2H, m, $H^{2,3}$), 3.00 (2H, m, $H^{1,4}$), 2.03 (3H, s, CH_3), 2.00 (3H, s, CH_3), 1.46 (1H, d, *J* 10.3 Hz, H^{7s}), 1.14 (1H, d, H^{7a}).

***N*-(*o*,*m*′-Dimethylphenyl)-*exo*-5,6-epoxybicyclo[2.2.1]heptan-*endo*,*endo*-2,3-dicarboximide (9g).** White solid; mp 193-195 °C; 5.25 g (92.7%) yield. R_f 0 (2-propanol). Found: C, 72.00; H, 6.02; N, 4.91. $C_{17}H_{17}NO_3$ requires: C, 72.08; H, 6.01; N, 4.95%. IR (KBr, cm^{-1}): 3050, 3015, 1762, 1708, 1370, 1190, 860. ^{1}H NMR (200 MHz) δ_H 7.24-7.13 (2H, m, H_{arom}), 6.94 (1H, s, H_{arom}), 3.49 (1H, dd, *J* 3.1, 1.5 Hz, H^5), 3.42 (1H, dd, H^6), 3.35 (2H, m, $H^{2,3}$), 2.97 (2H, m, $H^{1,4}$), 2.27 (3H, s, CH_3), 2.00 (3H, s, CH_3), 1.43 (1H, d, *J* 10.0 Hz, H^{7s}), 1.14 (1H, d, H^{7a}).

***N*-(*p*-Nitrophenyl)-*exo*-5,6-epoxybicyclo[2.2.1]heptan-*endo*,*endo*-2,3-dicarboximide (9l).** White solid; mp 249-251 °C; 4.45 g (74.2%) yield. R_f 0 (2-propanol). Found: C, 59.93; H, 4.06; N, 9.39. $C_{15}H_{12}N_2O_5$ requires: C, 60.00; H, 4.00; N, 9.33%. IR (KBr, cm^{-1}): 3040, 1775, 1710, 1523, 1496, 1348, 852. ^{1}H NMR (300 MHz, $CDCl_3$) δ_H 8.20 (2H, d, H_{arom}), 7.35 (2H, d, H_{arom}), 3.33 (2H, dd, $H^{5,6}$), 3.23 (2H, m, $H^{2,3}$), 3.13 (2H, m, $H^{1,4}$), 1.76 (1H, d, *J* 10.0 Hz, H^{7s}), 1.59 (1H, d, H^{7a}). ^{13}C NMR (100 MHz, $CDCl_3$) δ_C 175.98

 This journal is © The Royal Society of Chemistry 2010

(C=O), 148.31, 138.05, 128.09, 125.45 (C_{arom}), 48.30 ($C^{5,6}$), 46.76 ($C^{2,3}$), 40.72 ($C^{1,4}$), 30.41 (C^{7}).

***N*-(*p*-Ethoxycarbonylphenyl)-*exo*-5,6-epoxybicyclo[2.2.1]-heptan-*endo*,*endo*-2,3-dicarboximide (9m).** White solid; mp 204-206 °C; 6.21 g (94.9%) yield. R_f 0 (2-propanol). Found: C, 66.12; H, 5.29; N, 4.22. $C_{18}H_{17}NO_5$ requires: C, 66.06; H, 5.20; N, 4.28%. IR (KBr, cm^{-1}): 3035, 1720, 1690, 1605, 1520, 1390, 1180, 865. ^{1}H NMR (200 MHz) δ_H 8.04 (2H, d, H_{arom}), 7.46 (2H, d, H_{arom}), 4.33 (2H, q, CH_2), 3.42 (2H, m, $H^{5,6}$), 3.34 (2H, m, $H^{2,3}$), 2.97 (2H, m, $H^{1,4}$), 1.41 (1H, d, *J* 10.4 Hz, H^{7s}), 1.32 (3H, t, CH_3), 1.14 (1H, d, H^{7a}).

***N*-(2-Thiadiazolyl)-*exo*-5,6-epoxybicyclo[2.2.1]heptan-*endo*,*endo*-2,3-dicarboximide (9n).** White solid; mp 203-205 °C; 2.18 g (41.4%) yield. R_f 0.14 (diethyl ether), 0.53 (2-propanol). Found: C, 50.26; H, 3.50; N, 15.89. $C_{11}H_9N_3O_3S$ requires: C, 50.19; H, 3.42; N, 15.97%. IR (KBr, cm^{-1}): 3065, 1794, 1728, 1462, 1346, 1200, 851. ^{1}H NMR (200 MHz) δ_H 9.65 (1H, s, H_{arom}), 3.53 (1H, dd, *J* 3.2, 1.5 Hz, H^5), 3.52 (1H, dd, H^6), 3.23 (2H, m, $H^{2,3}$), 3.02 (2H, m, $H^{1,4}$), 1.41 (1H, d, *J* 10.5 Hz, H^{7s}), 1.17 (1H, d, H^{7a}).

***N*-Cyclohexyl-*exo*-5,6-epoxybicyclo[2.2.1]heptan-*endo*,*endo*-2,3-dicarboximide (9o).** White solid; mp 202-204 °C; 4.90 g (93.8%) yield. R_f 0 (2-propanol). Found: C, 69.06; H, 7.35; N, 5.30. $C_{15}H_{19}NO_3$ requires: C, 68.97; H, 7.28; N, 5.36%. IR (KBr, cm^{-1}): 3050, 1760, 1700, 1380, 1190, 860. ^{1}H NMR (200 MHz) δ_H 3.79 (1H, tt, CH_{cycl}), 3.18 (1H, dd, *J* 3.2, 1.1 Hz, H^5), 3.17 (1H, dd, H^6), 3.07 (2H, m, $H^{2,3}$), 2.86 (2H, m, $H^{1,4}$), 1.93-2.07 (2H, H_{cycl}), 1.47-1.76 (5H, H_{cycl}), 1.34 (1H, d, *J* 10.1 Hz, H^{7s}), 1.06-1.25 (3H, H_{cycl}), 1.02 (1H, d, H^{7a}).

General procedure for the synthesis of compounds (10a–e, 11e–k, 12j–o)

A solution of 1.0 M sodium ethoxide (0.005 mol, 5 mL) was added to a suspension of epoxyimide (**9a–p**) (0.005 mol) in 4–5 mL absolute ethanol at room temperature. The reaction mixture was stirred. The completion of reaction was monitored by TLC. The resulting clear solution was cooled to 0 °C, the 20% solution of HCl was added gradually to the reaction mixture up to pH 6. The formed residue was filtered out, washed with ice water, dried and purified by crystallization from 2-propanol.

If the residue was not generated (for example, *trans*-dihydroximides (**10a**,**b**), which are soluble in water), the reaction mixture was evaporated. The dried compound was treated by "boiling" acetone, sodium chloride was filtered out. The filtrate was dried and purified by crystallization from 2-propanol or acetone.

***N*-Methyl-*exo*-2,*endo*-3-dihydroxybicyclo[2.2.1]heptan-*endo*,*endo*-2,3-dicarboximide (10a).** White solid; mp 184-186 °C; 0.80 g (76.3%) yield. R_f 0.60 (2-propanol). Found: C, 56.79; H, 6.29; N, 6.58. $C_{10}H_{13}NO_4$ requires: C, 56.86; H, 6.20; N, 6.63%. IR (KBr, cm^{-1}): 3415, 3295, 1760, 1685, 1450. ^{1}H NMR (300 MHz) δ_H 4.96 (1H, d, OH), 4.92 (1H, d, OH), 3.72 (1H, s, H^3), 3.18 (1H, dd, H^6), 3.15 (1H, s, H^2), 2.92 (1H, dd, *J* 9.5, 4.5 Hz, H^5), 2.71 (3H, s, CH_3), 2.62 (1H, m, H^4), 2.33 (1H, d, *J* 6.2, H^1), 1.83 (1H, d, *J* 10.4 Hz, H^{7s}), 1.43 (1H, d, H^{7a}). MS (EI, 70 eV): *m*/*z* (relative intensity) = 211 (M^+, 57), 193 (73), 165 (65), 126 (36), 112 (100), 108 (24), 100 (7).

***N*-*n*-Propyl-*exo*-2,*endo*-3-dihydroxybicyclo[2.2.1]heptan-*endo*,*endo*-2,3-dicarboximide (10b).** White solid; mp 142-145 °C; 1.15 g (96.2%) yield. R_f 0.12 (ether), 0.67 (2-propanol). Found: C, 60.29; H, 7.21; N, 5.92. $C_{12}H_{17}NO_4$ requires: C, 60.24; H, 7.16; N, 5.85%. IR (KBr, cm^{-1}): 3475, 3430, 1740, 1680, 1410. ^{1}H NMR (300 MHz) δ_H 5.00 (1H, s, OH), 4.95 (1H, s, OH), 3.72 (1H, d, *J* 3.6 Hz, H^3), 3.22 (1H, dd, H^6), 3.20 (2H, t, CH_2), 3.17 (1H, s, H^2), 2.92 (1H, dd, *J* 9.3, 5.1 Hz, H^5), 2.61 (1H, m, H^4), 2.33 (1H, d, *J* 5.7, H^1), 1.83 (1H, d, *J* 10.5 Hz, H^{7s}), 1.45 (2H, m, CH_2), 1.42 (1H, d, H^{7a}), 0.83 (3H, t, CH_3).

***N*-*i*-Propyl-*exo*-2,*endo*-3-dihydroxybicyclo[2.2.1]heptan-*endo*,*endo*-2,3-dicarboximide (10c).** White solid; mp 130-133 °C; 1.00 g (84.1%) yield. R_f 0.64 (2-propanol). Found: C, 60.30; H, 7.07; N, 5.89. $C_{12}H_{17}NO_4$ requires: C, 60.24; H, 7.16; N, 5.85%. IR (KBr, cm^{-1}): 3450, 3320, 1765, 1680, 1415. ^{1}H NMR (300 MHz) δ_H 5.06 (1H, s, OH), 4.87 (1H, s, OH), 4.12 (1H, m, CH), 3.72 (1H, s, H^3), 3.21 (1H, s, H^2), 3.09 (1H, dd, H^6), 2.87 (1H, dd, *J* 9.4, 4.7 Hz, H^5), 2.60 (1H, m, H^4), 2.38 (1H, d, *J* 6.0, H^1), 1.82 (1H, d, *J* 9.9 Hz, H^{7s}), 1.39 (1H, d, H^{7a}), 1.25 (6H, d, $2CH_3$).

***N*-Benzyl-*exo*-2,*endo*-3-dihydroxybicyclo[2.2.1]heptan-*endo*,*endo*-2,3-dicarboximide (10d).** White solid; mp 127-130 °C; 1.27 g (88.5%) yield. R_f 0.12 (2-propanol). Found: C, 66.81; H, 5.89; N, 4.91. $C_{16}H_{17}NO_4$ requires: C, 66.89; H, 5.96; N, 4.88%. IR (KBr, cm^{-1}): 3505, 3420, 1780, 1710, 1600, 1515, 785, 745, 715. ^{1}H NMR (300 MHz) δ_H 7.23-7.30 (5H, H_{arom}), 5.09 (1H, s, OH), 4.99 (1H, s, OH), 4.51 (1H, d, *J* 14.9, CH), 4.36 (1H, d, CH), 3.77 (1H, d, *J* 4.5, H^3), 3.27 (1H, dd, H^6), 3.21 (1H, s, H^2), 3.02 (1H, dd, *J* 9.5, 4.7 Hz, H^5), 2.65 (1H, m, H^4), 2.35 (1H, d, *J* 5.8, H^1), 1.85 (1H, d, *J* 10.1 Hz, H^{7s}), 1.44 (1H, d, H^{7a}).

***N*-Cyclohexyl-*exo*-2,*endo*-3-dihydroxybicyclo[2.2.1]heptan-*endo*,*endo*-2,3-dicarboximide (10e).** White solid; mp 204-206 °C; 0.46 g (32.8%) yield. R_f 0.87 (2-propanol). Found: C, 64.43; H, 7.64; N, 4.91. $C_{15}H_{21}NO_4$ requires: C, 64.52; H, 7.53; N, 5.02%. IR (KBr, cm^{-1}): 3435, 3350, 1750, 1680, 1455, 1405, 1205, 1070. ^{1}H NMR (300 MHz) δ_H 5.01 (1H, s, OH), 4.95 (1H, s, OH), 3.77 (1H, m, CH_{cycl}), 3.72 (1H, d, *J* 3.3, H^3), 3.20 (1H, s, H^2), 3.09 (1H, dd, H^6), 2.87 (1H, dd, *J* 9.8, 5.0 Hz, H^5), 2.60 (1H, m, H^4), 2.31 (1H, d, *J* 5.9, H^1), 1.88-2.09 (2H, H_{cycl}), 1.81 (1H, d, *J* 10.5 Hz, H^{7s}), 1.71-1.75 (2H, H_{cycl}), 1.48-1.61 (3H, H_{cycl}), 1.39 (1H, d, H^{7a}), 1.06-1.28 (3H, H_{cycl}).

***N*-*n*-Tolyl-*exo*-2-hydroxy-5-oxo-4-oxatricyclo[4.2.1.$0^{3,7}$]nonane-*endo*-9-carboxamide (11e).** White solid; mp 219-221 °C; 1.19 g (83.1%) yield. R_f 0.71 (2-propanol). Found: C, 66.75; H, 5.99; N, 4.81. $C_{16}H_{17}NO_4$ requires: C, 66.89; H, 5.92; N, 4.88%. IR (KBr, cm^{-1}): 3330, 3315, 1765, 1675, 1605, 1540, 1520, 1410, 1255, 1170, 1030, 830. ^{1}H NMR (300 MHz) δ_H 9.99 (1H, s, NH), 7.42 (2H, d, H_{arom}), 7.09 (2H, d, H_{arom}), 5.14 (1H, s, OH), 4.34 (1H, d, *J* 3.6 Hz, H^3), 4.29 (1H, s, H^2), 3.23 (1H, m, H^7), 3.05 (1H, dd, *J* 10.4, 3.0 Hz, H^9), 2.69 (1H, dd, *J* 4.5 Hz, H^6), 2.46 (1H, s, H^1), 2.24 (3H, s, CH_3), 2.02 (1H, d, H^{8s}), 1.48 (1H, d, *J* 10.7 Hz, H^{8a}). MS (EI, 70 eV): *m*/*z* (relative intensity) = 287 (M^+, 38), 206 (17), 188 (16), 108 (26), 107 (100), 82 (4), 65 (7).

***N*-*o*,*o*′-Dimethylphenyl-*exo*-2-hydroxy-5-oxo-4-oxatricyclo-[4.2.1.$0^{3,7}$]nonane-*endo*-9-carboxamide (11f).** White solid; mp 220-222 °C; 1.16 g (77.0%) yield. R_f 0.76 (2-propanol). Found: C, 67.69; H, 6.43; N, 4.71. $C_{17}H_{19}NO_4$ requires: C, 67.76; H, 6.36;

N, 4.65%. IR (KBr, cm^{-1}): 3520, 3345, 1740, 1678, 1600, 1520, 1380, 1235, 1170, 1028, 890. ^1H NMR (300 MHz) δ_H 9.45 (1H, s, NH), 7.05 (3H, m, H_{arom}), 5.18 (1H, s, OH), 4.31 (1H, d, *J* 5.1 Hz, H^3), 4.28 (1H, s, H^2), 3.23 (1H, m, H^7), 3.15 (1H, dd, *J* 10.6, 3.0 Hz, H^9), 2.70 (1H, dd, *J* 4.7 Hz, H^6), 2.50 (1H, s, H^1), 2.14 (6H, s, $2CH_3$), 2.02 (1H, d, H^{8s}), 1.52 (1H, d, *J* 10.5 Hz, H^{8a}).

***N*-*o*,*m*′-Dimethylphenyl-*exo*-2-hydroxy-5-oxo-4-oxatricyclo-[4.2.1.0^{3,7}]nonane-*endo*-9-carboxamide (11g).** White solid; mp 217-219 °C; 1.30 g (86.6%) yield. R_f 0.12 (ether), 0.79 (2-propanol). Found: C, 67.83; H, 6.28; N, 4.70. $C_{17}H_{19}NO_4$ requires: C, 67.76; H, 6.36; N, 4.65%. IR (KBr, cm^{-1}): 3515, 3330, 1758, 1665, 1580, 1550, 1495, 1395, 1270, 1170, 1020, 888, 820. ^1H NMR (300 MHz) δ_H 9.37 (1H, s, NH), 7.16 (1H, s, H_{arom}), 7.07 (1H, d, H_{arom}), 6.89 (1H, d, H_{arom}), 5.17 (1H, s, OH), 4.33 (1H, d, *J* 5.7 Hz, H^3), 4.30 (1H, s, H^2), 3.23 (1H, m, H^7), 3.15 (1H, dd, *J* 10.5, 3.0 Hz, H^9), 2.72 (1H, dd, *J* 4.5 Hz, H^6), 2.49 (1H, s, H^1), 2.24 (3H, s, CH_3), 2.15 (3H, s, CH_3), 2.02 (1H, d, H^{8s}), 1.49 (1H, d, *J* 10.7 Hz, H^{8a}).

***N*-*n*-Methoxyphenyl-*exo*-2-hydroxy-5-oxo-4-oxatricyclo-[4.2.1.0^{3,7}]nonane-*endo*-9-carboxamide (11h).** White solid; mp 168-170 °C; 0.87 g (57.6%) yield. R_f 0.62 (2-propanol). Found: C, 63.28; H, 5.73; N, 4.55. $C_{16}H_{17}NO_5$ requires: C, 63.36; H, 5.65; N, 4.62%. IR (KBr, cm^{-1}): 3480, 3330, 1755, 1665, 1610, 1552, 1520, 1400, 1260, 1175, 1030, 840. ^1H NMR (300 MHz) δ_H 9.94 (1H, s, NH), 7.44 (2H, d, H_{arom}), 6.87 (2H, d, H_{arom}), 5.14 (1H, s, OH), 4.33 (1H, d, *J* 5.7 Hz, H^3), 4.30 (1H, s, H^2), 3.71 (3H, s, OCH_3), 3.23 (1H, m, H^7), 3.07 (1H, dd, *J* 10.4, 3.0 Hz, H^9), 2.69 (1H, dd, *J* 5.1 Hz, H^6), 2.45 (1H, s, H^1), 2.01 (1H, d, H^{8s}), 1.48 (1H, d, *J* 10.8 Hz, H^{8a}).

***N*-*n*-Bromophenyl-*exo*-2-hydroxy-5-oxo-4-oxatricyclo[4.2.1.0^{3,7}]nonane-*endo*-9-carboxamide (11i).** White solid; mp 116-119 °C; 1.67 g (94.9%) yield. R_f 0.33 (ether), 0.71 (2-propanol). Found: C, 51.25; H, 3.97; N, 3.99. $C_{15}H_{14}NO_4Br$ requires: C, 51.16; H, 4.01; N, 3.98%. IR (KBr, cm^{-1}): 3490, 3320, 1760, 1680, 1600, 1540, 1495, 1400, 1250, 1170, 1030, 835. ^1H NMR (300 MHz) δ_H 10.24 (1H, s, NH), 7.52 (2H, d, H_{arom}), 7.47 (2H, d, H_{arom}), 5.17 (1H, s, OH), 4.34 (1H, d, *J* 4.8 Hz, H^3), 4.26 (1H, s, H^2), 3.24 (1H, m, H^7), 3.07 (1H, dd, *J* 10.6, 3.6 Hz, H^9), 2.72 (1H, dd, *J* 5.0 Hz, H^6), 2.47 (1H, s, H^1), 2.02 (1H, d, H^{8s}), 1.49 (1H, d, *J* 10.7 Hz, H^{8a}).

***N*-Cyclohexyl-*exo*-2-hydroxy-5-oxo-4-oxatricyclo[4.2.1.0^{3,7}]-nonane-*endo*-9-carboxamide (11j).** White solid; mp 173-175 °C; 0.11 g (8.2%) yield. R_f 0 (2-propanol). Found: C, 64.59; H, 7.44; N, 5.09. $C_{15}H_{21}NO_4$ requires: C, 64.52; H, 7.53; N, 5.02%. IR (KBr, cm^{-1}): 3510, 3300, 1755, 1655, 1555, 1380, 1210, 1170, 1020. ^1H NMR (300 MHz) δ_H 7.83 (1H, d, *J* 7.2 Hz, NH), 5.00 (1H, s, OH), 4.29 (1H, d, *J* 5.0 Hz, H^3), 4.26 (1H, s, H^2), 3.73 (1H, m, CH_{cycl}), 3.16 (1H, m, H^7), 2.81 (1H, dd, *J* 10.0, 3.8 Hz, H^9), 2.56 (1H, dd, *J* 5.1 Hz, H^6), 2.50 (1H, s, H^1), 1.96 (1H, d, H^{8s}), 1.80-2.03 (2H, H_{cycl}), 1.49-1.76 (5H, H_{cycl}), 1.39 (1H, d, *J* 10.1 Hz, H^{8a}), 1.06-1.27 (3H, H_{cycl}).

***N*-(6-Quinolyl)-*exo*-2-hydroxy-5-oxo-4-oxatricyclo[4.2.1.0^{3,7}]-nonane-*endo*-9-carboxamide (11k).** Light green solid; mp 185-187 °C (dec); 0.38 g (23.6%) yield. R_f 0.64 (2-propanol). Found: C, 66.71; H, 4.99; N, 8.72. $C_{18}H_{16}N_2O_4$ requires: C, 66.67; H, 4.94; N, 8.64%. IR (KBr, cm^{-1}): 3400, 3280, 1762, 1690, 1618, 1570, 1420, 1378, 1255, 1212, 1190, 1025. ^1H NMR (300 MHz) δ_H 11.22 (1H, s, NH), 9.14 (1H, d, H_{arom}), 9.07 (1H, d, H_{arom}), 8.74 (1H, s, H_{arom}), 8.38 (1H, d, H_{arom}), 8.17 (1H, dd, H_{arom}), 7.99 (1H, dd, H_{arom}), 5.50 (1H, s, OH), 4.40 (1H, d, *J* 5.1 Hz, H^3), 3.63 (1H, s, H^2), 3.24 (1H, m, H^7), 2.99 (1H, m, H^9), 2.65 (1H, m, H^6), 2.50 (1H, s, H^1), 1.92 (1H, d, H^{8s}), 1.74 (1H, d, *J* 10.4 Hz, H^{8a}).

***N*-Phenyl-*exo*-2-hydroxy-5-oxo-4-azatricyclo[4.2.1.0^{3,7}]nonane-*endo*-9-carboxylic acid (12j).** White solid; mp 250-252 °C; 1.09 g (79.9%) yield. R_f 0.86 (2-propanol). Found: C, 65.81; H, 5.50; N, 5.19. $C_{15}H_{15}NO_4$ requires: C, 65.92; H, 5.53; N, 5.13%. IR (KBr, cm^{-1}): 3485, 1725, 1665, 1595, 1500, 1415, 1190, 770, 705. ^1H NMR (300 MHz) δ_H 12.26 (1H, s, COOH), 7.61 (2H, d, H_{arom}), 7.36 (2H, t, H_{arom}), 7.10 (1H, t, H_{arom}), 5.24 (1H, s, OH), 4.21 (1H, s, H^2), 3.81 (1H, d, *J* 5.1 Hz, H^3), 3.10 (1H, m, H^7), 2.99 (1H, dd, *J* 10.5, 2.9 Hz, H^9), 2.69 (1H, dd, *J* 4.1 Hz, H^6), 2.47 (1H, s, H^1), 2.00 (1H, d, H^{8s}), 1.45 (1H, d, *J* 9.9 Hz, H^{8a}).

***N*-*m*-Nitrophenyl-*exo*-2-hydroxy-5-oxo-4-azatricyclo[4.2.1.0^{3,7}]-nonane-*endo*-9-carboxylic acid (12k).** Yellow solid; mp 235-237 °C; 1.29 g (81.0%) yield. R_f 0.77 (2-propanol). Found: C, 56.66; H, 4.37; N, 8.89. $C_{15}H_{14}N_2O_6$ requires: C, 56.60; H, 4.43; N, 8.80%. IR (KBr, cm^{-1}): 3495, 1760, 1700, 1580, 1545, 1495, 1405, 1360, 1230, 1150, 1072, 890, 818. ^1H NMR (300 MHz) δ_H 12.36 (1H, s, COOH), 8.72 (1H, s, H_{arom}), 7.97 (1H, d, H_{arom}), 7.85 (1H, d, H_{arom}), 7.69 (1H, m, H_{arom}), 5.35 (1H, s, OH), 4.15 (1H, s, H^2), 3.97 (1H, d, *J* 5.1 Hz, H^3), 3.15 (1H, m, H^7), 3.05 (1H, dd, *J* 10.5, 3.9 Hz, H^9), 2.76 (1H, dd, *J* 4.8 Hz, H^6), 2.50 (1H, s, H^1), 2.04 (1H, d, H^{8s}), 1.51 (1H, d, *J* 10.4 Hz, H^{8a}). MS (EI, 70 eV): *m*/*z* (relative intensity) = 318 (M^+, 22), 301 (4), 290 (11), 245 (16), 243 (20), 205 (100).

***N*-*p*-Nitrophenyl-*exo*-2-hydroxy-5-oxo-4-azatricyclo[4.2.1.0^{3,7}]-nonane-*endo*-9-carboxylic acid (12l).** Yellow solid; mp 192-194 °C; 1.33 g (83.6%) yield. R_f 0.76 (2-propanol). Found: C, 56.57; H, 4.40; N, 8.73. $C_{15}H_{14}N_2O_6$ requires: C, 56.60; H, 4.43; N, 8.80%. IR (KBr, cm^{-1}): 3490, 1720, 1680, 1590, 1520, 1375, 1335, 1310, 1270, 1225, 1195, 1120, 1055, 805. ^1H NMR (200 MHz) δ_H 12.24 (1H, s, COOH), 8.26 (2H, d, H_{arom}), 7.86 (2H, d, H_{arom}), 5.40 (1H, s, OH), 4.10 (1H, s, H^2), 3.97 (1H, d, *J* 5.2 Hz, H^3), 3.14 (1H, m, H^7), 3.05 (1H, dd, *J* 10.7, 3.4 Hz, H^9), 2.76 (1H, dd, *J* 4.6 Hz, H^6), 2.50 (1H, s, H^1), 2.04 (1H, d, H^{8s}), 1.51 (1H, d, *J* 10.8 Hz, H^{8a}).

***N*-*p*-Ethoxycarbonylphenyl-*exo*-2-hydroxy-5-oxo-4-azatricyclo-[4.2.1.0^{3,7}]nonane-*endo*-9-carboxylic acid (12m).** White solid; mp 235-237 °C; 1.19 g (69.0%) yield. R_f 0.84 (2-propanol). Found: C, 62.70; H, 5.43; N, 4.13. $C_{18}H_{19}NO_6$ requires: C, 62.61; H, 5.51; N, 4.06%. IR (KBr, cm^{-1}): 3400, 1770, 1695, 1600, 1535, 1410, 1300, 1255, 1180, 1120, 1020, 820. ^1H NMR (300 MHz) δ_H 7.93 (2H, d, H_{arom}), 7.74 (2H, d, H_{arom}), 4.54 (1H, s, OH), 4.29 (2H, q, CH_2), 4.17 (1H, s, H^2), 3.87 (1H, d, *J* 4.2 Hz, H^3), 3.10 (1H, m, H^7), 2.98 (1H, dd, *J* 10.6, 3.2 Hz, H^9), 2.72 (1H, dd, *J* 3.9 Hz, H^6), 2.47 (1H, s, H^1), 2.08 (1H, d, H^{8s}), 1.49 (1H, d, *J* 10.2 Hz, H^{8a}), 1.34 (3H, t, CH_3).

***N*-(2-Thiadiazolyl)-*exo*-2-hydroxy-5-oxo-4-azatricyclo[4.2.1.0^{3,7}]nonane-*endo*-9-carboxylic acid (12n).** White solid; mp 234-236 °C (dec); 1.19 g (61.5%) yield. R_f 0.68 (2-propanol). Found: C, 47.07; H, 3.99; N, 14.18. $C_{11}H_{11}N_3O_4S$ requires: C, 46.98; H, 3.91; N, 14.95%. IR (KBr, cm^{-1}): 3630, 3450, 1770, 1722, 1618, 1500, 1345, 1255, 1225, 1160, 1055. ^1H NMR (300 MHz) δ_H 12.73

 This journal is © The Royal Society of Chemistry 2010

Table 5 The crystallographic data and experimental parameters for compounds **10a**, **11e**, **12k**

Parameter	**10a**	**11e**	**12k**
Formula	$C_{10}H_{13}NO_4$	$C_{16}H_{17}NO_4 \cdot C_3H_8O$	$C_{15}H_{14}N_2O_6$
Unit cell dimensions			
a/Å	11.2977(16)	11.5561(15)	7.2192(13)
b/Å	6.6557(9)	11.7060(16)	9.064(2)
c/Å	13.778(2)	27.578(3)	11.0633(16)
α (°)	90	90	73.995(18)
β (°)	111.676(13)	90	80.033(14)
γ (°)	90	90	73.38(2)
V/Å^3	962.8(2)	3730.6(8)	663.3(2)
T/K	293	293	100
F(000)	448	1488	332
Crystal system	Monoclinic	Orthorhombic	Triclinic
Space group	$P2_1/c$	$Pbca$	$P\bar{1}$
Z	4	8	2
μ/mm^{-1}	0.113	0.089	0.125
D_c/g cm^{-3}	1.457	1.237	1.594
$2\Theta_{max}$/grad	55	60	55
Measured reflections	4844	29562	4837
Independent reflections	2198	5427	2981
R_{int}	0.014	0.059	0.016
Reflections with $F>4\sigma(F)$	1874	2335	2473
R_1	0.035	0.070	0.034
wR_2	0.099	0.201	0.093
S	1.075	0.882	1.076
CCDC	706778	706779	706780

(1H, s, COOH), 9.26 (1H, s, H_{arom}), 5.45 (1H, s, OH), 4.37 (1H, d, J 5.1 Hz, H^3), 3.61 (1H, s, H^2), 3.18 (1H, m, H^7), 2.99 (1H, m, H^9), 2.66 (1H, m, H^6), 2.60 (1H, s, H^1), 1.99 (1H, d, H^{8s}), 1.49 (1H, d, J 11.0 Hz, H^{8a}).

***N*-(6-Quinolyl)-*exo*-2-hydroxy-5-oxo-4-azatricyclo[4.2.1.0^{3,7}]-nonane-*endo*-9-carboxylic acid (12o).** Light green solid; mp 273-275 °C; 0.46 g (28.3%) yield. R_f 0.44 (2-propanol). Found: C, 66.75; H, 5.01; N, 8.55. $C_{18}H_{16}N_2O_4$ requires: C, 66.67; H, 4.94; N, 8.64%. IR (KBr, cm^{-1}): 3400, 1730, 1710, 1615, 1495, 1395, 1355, 1190, 1070. ^{1}H NMR (200 MHz) δ_H 9.08 (1H, dd, H_{arom}), 9.00 (1H, d, H_{arom}), 8.56 (1H, dd, H_{arom}), 8.35 (1H, d, H_{arom}), 8.32 (1H, s, H_{arom}), 7.90 (1H, dd, H_{arom}), 5.10 (1H, s, OH), 4.24 (1H, s, H^2), 4.06 (1H, d, J 5.0 Hz, H^3), 3.19 (1H, m, H^7), 3.07 (1H, dd, J 10.5, 3.2 Hz, H^9), 2.79 (1H, dd, J 4.4 Hz, H^6), 2.50 (1H, s, H^1), 2.08 (1H, d, H^{8s}), 1.52 (1H, d, J 10.5 Hz, H^{8a}).

The X-ray diffraction study

All experiments were carried out on the "Xcalibur-3" diffractometer (graphite monochromated Mo-Kα radiation, CCD detector, ω-scaning). The structures were solved by direct methods using the SHELXTL package.[25] Crystallographic data and parameters of experiments are listed in Table 5.

The positions of the hydrogen atoms were located from electron density difference maps for all structures and refined by the "riding" model with $U_{iso} = nU_{eq}$ of the carrier atom (n = 1.5 for methyl and hydroxyl groups and n = 1.2 for other hydrogen atoms) for the structure **11e**. The positions of the hydrogen atoms in the structures **10a** and **12k** were refined in isotropic approximation. All non-hydrogen atoms were refined using anisotropic approximation. The final atomic coordinates, and crystallographic data have been deposited with the Cambridge Crystallographic Data Centre, 12 Union Road, CB2 1EZ, UK (fax: +44-1223-336033; e-mail: deposit@ccdc.cam.ac.uk).

Calculations

All computations were carried out with the Gaussian 03 program package.[26] Geometry optimizations of the local minima and transition state structures were performed using the B3LYP functional[27] and the 6-31+G(d)[28] basis set in the presence of ethanol as solvent (Polarizable Continuum Model (PCM)). The basis set includes diffuse functions on heavy atoms to ensure the appropriate description of the anionic reactants.[29] Harmonic vibrational frequencies and zero-point vibrational energy (ZPVE) corrections were calculated at the same level of theory. All of the transition states are characterized by just one imaginary frequency, in all cases greater than 100i cm^{-1}. In the PCM approach, the solute molecule was embedded in a cavity in a dielectric medium *via* a series of overlapping spheres that represents the solvent.[30] Solute–solvent interactions were described by a reaction potential arising from the presence of the dielectric medium. The United Atom Topological Model (UA0) was used for building up the solvent cavity.

The energies of optimized structures were corrected by (ZPVE) scaled by 0.98.[31] The dielectric constant ($\varepsilon = 24.55$) which formally corresponds to the bulk of ethanol has been used. The computed enthalpy and Gibbs free energy were converted from 1 atm standard state into the standard state of molar concentration (ideal mixture mol L^{-1} and 1 atm) in order to allow a direct comparison with the experimental result in solution.[32]

The kinetic simulations were performed using the kTSim program.[33] The rate constants for the considered steps of ethanolysis reactions were estimated using standard Transition State Theory[34] in the following form:

$$k = \frac{k_b T}{h} \exp\left(-\frac{\Delta G^{\ddagger}}{RT}\right) \quad (1)$$

Where $\Delta G^{\ddagger}$ - activation Gibbs free energy for the reaction, T-temperature, k_b- Boltzmann's constant, h - Plank's constant, R - universal gas constant. The equilibrium constants were calculated using standard equation: $K = \exp\left(-\frac{\Delta G}{RT}\right)$, where ΔG - is the relative total Gibbs free energy of the reactant and product, T-temperature, R - universal gas constant.

Acknowledgements

This work was supported in part by the National Science Foundation through EPSCoR grant No. 440900 362427-02 and by the Ukrainian Fundamental Researches State Fund Grant F 25.3/067. We thank the Mississippi Center for Supercomputer Research for a generous allotment of computer time.

References

1 (*a*) F. Csende, F. Fulop and G. Stajer, *Curr. Org. Synth.*, 2008, **5**, 173–185; (*b*) D. Rennison, S. Bova, M. Cavalli, F. Ricchelli, A. Zulian, B. Hopkins and M. A. Brimble, *Bioorg. Med. Chem.*, 2007, **15**,

2963–2974; (*c*) E. E. Parent, C. S. Dence, T. L. Sharp, M. J. Welch and J. A. Katzenellenbogen, *Nucl. Med. Biol.*, 2006, **33**, 615–624; (*d*) I. I. Kiseleva, N. G. Perminova, O. A. Liasunova, D. I. Timofeev, A. V. Serbin, L. I. Kasyan, I. A. Egorov, T. S. Grebinik and I. V. Timofeev, *Molekuliarnaia genetika, mikrobiologiia i virusologiia*, 2005, **2**, 33–36; (*e*) H. D. Maynard, S. Y. Okada and R. H. Grubbs, *J. Am. Chem. Soc.*, 2001, **123**, 1275–1279; (*f*) A. Casini, F. Mincione, M. A. Ilies, L. Menabuoni, A. Scozzafava and C. T. Supuran, *J. Enzyme Inhib. Med. Chem.*, 2001, **16**, 113–123; (*g*) D. A. Brown, K. Lesiak, W.-Y. Ren, K. L. Strezelecki and A. A. Khorlin, *Pigm. Cell Res.*, 1999, **12**, 36–47; (*h*) D. A. Brown, W.-Y. Ren, A. A. Khorlin, K. Lesiak, D. Conklin, K. A. Watanabe, M. M. Seidman and J. George, *J. Invest. Dermatol.*, 1998, **110**, 428–437; (*i*) W. Jaeger, B. Paesler, G. Buchbauer and P. Chiba, *Pharmazie.*, 1995, **50**, 619–621; (*j*) G. Buchbauer, H. Spreitzer and B. Schwayer, *Parfuemerie und Kosmetik*, 1992, **73**, pp. 146, 148-150, 153; (*k*) T. Wasaki, H. Yamazaki, T. Nishitani and T. Sato, *Chem. Pharm. Bulletin*, 1991, **39**, 527–529; (*l*) R. Lesyk, B. Zimenkovsky, D. Atamanyuk, F. Jensen, K. Kiecr-Kononowiczc and A. Gzellad, *Bioorg. Med. Chem.*, 2006, **14**, 5230–5240; (*m*) L. R. Makings, D. R. Hurley, M. Garcia-Guzman Blanco, D. J. Bergeron and A. Nakatani, *WO Pat.*, 2005117883 A1, 2005; (*n*) D. Atamanyuk, B. Zimenkovsky and R. Lesyk, *J. Sulfur Chem.*, 2008, **29**, 151–162; (*o*) E. E. Parent, C. S. Dence, T. L. Sharp, M. J. Welch and J. A. Katzenellenbogen, *Nucl. Med. Biol.*, 2006, **33**, 615–624; (*p*) J Obniska, R Lesyk, D Atamanyuk and K Kaminski, *Acta Polon. Pharm.*, 2005, **62**, 213–219; (*q*) K. A. Scappaticci, *US Pat.*, 5011841 A, 1991; (*r*) H. Zlenko, L. Kasyan, V. Mamchur, A. Kasyan, H. Podpletnjaja, I. Tarabara and O. Krishchik, Abstr. of Papers of 2nd European Congress of Pharmacology, Budapest, Hungary, *Fund. Clin. Pharm.*, 1999, **13**, 377; (*s*) I. Matuo, *US Pat*., 3850922, 1974; (*t*) D. V. Petrov, V. A. Gorpinchenko, E. A. Shafikova, F. S. Zarudii, N. Z. Baschenko, R. Y. Khisamutdinova, N. S. Makara, V. A. Vakhitov, Y. V. Vakhitova, W. M. Chang, R.I. Alimbekov, V. A. Dokichev, Y. V. Tomilov and O. M. Nefedov, *RU Pat.*, 2281938 C1, 2006; (*u*) M. Takaya, K. Ozeki, H. Tanizawa and M. Sato, *JP Pat.*, 54103864, 1979; (*v*) A. G. Gasanov, E. G. Mamedov, I. G. Ayubov, S. T. Alieva, T. A. Samedova and G. Dzh. Gasanova, *Azerbaidzhanskii Khimicheskii Zhurnal.*, 2005, **3**, 88–91; (*w*) R. Jaehrling, P. Henklein, P. Scharfenberg, H. Teubner and G. Steimecke, *DD Pat*., 295630 A5, 1991; (*x*) P. Scharfenberg, P. Henklein, R. Jaehrling, P. Henklein, H. Teubner and G. Steimecke, *DD Pat*., 279875 A1, 1990.

2 (*a*) T. Eren, A. Som, J. R. Rennie, C. F. Nelson, Y. Urgina, K. Nüsslein, E. B. Coughlin and G. N. Tew, *Macromol. Chem. Phys.*, 2008, **209**, 516–524; (*b*) M. F. Ilker, K. Nüsslein, G. N. Tew and E. B. Coughlin, *J. Am. Chem. Soc.*, 2004, **126**, 15870–15875; (*c*) G. J. Gabriel, A. E. Madkour, J. M. Dabkowski, C. F. Nelson, K. Nüsslein and G. N. Tew, *Biomacromolecules*, 2008, **9**, 2980–2983; (*d*) Z. M. AL-Badri, A. Som, S. Lyon, C. F. Nelson, K. Nüsslein and G. N. Tew, *Biomacromolecules*, 2008, **9**, 2805–2810.

3 (*a*) E. Sidoova, Z. Olderova, A. Perjessy and G. Bloockinger, *Chem. Zvesti*, 1980, **34**, 269–277; (*b*) G. Buchbauer and A. M. Weck, *Chemiker-Zeitung.*, 1985, **109**, 255–265; (*c*) K. Muto, S. Ochiai and K. Kashima, *JP Pat*., 2000044846 A, 2000.

4 (*a*) L. I. Kasyan, A. O. Kasyan, S. I. Okovytyy and I. N. Tarabara, *Alicyclic Epoxidic Compounds. The reaction ability*, Dnepropetrovsk National University Press, Dnepropetrovsk, 2003, p.516; (*b*) L. Kasyan, A. Kasyan and S. Okovytyy, *Russ. J. Org. Chem*, 2004, **40**, 11–42; (*c*) L. I. Kasyan, I. N. Tarabara and A. O. Kasyan, *Russ. J. Org. Chem.*, 2004, **40**, 1227–1257; (*d*) O. V. Salomatina, O. I. Yarovaya and V. A. Barkhash, *Russ. J. Org. Chem.*, 2005, **41**, 156–188; (*e*) L. I. Kasyan, A. O. Kasyan and S. I. Okovytyy, *Russ. J. Org. Chem.*, 2006, **42**, 327–354; (*f*) I. Paterson, K. Fessner, M. Finlay, V. Raymond and M. F. Jacobs, *Tetrahedron Lett.*, 1996, **37**, 8803–8806; (*g*) S. Kanoh, M. Naka, T. Nishimura and M. Motoi, *Tetrahedron*, 2002, **58**, 7049–7064.

5 (*a*) J. A. Berson and S. Suzuki, *J. Am. Chem. Soc.*, 1958, **80**, 4341–4345; (*b*) Yu. K. Yur'ev and N. S. Zefirov, *Zhurnal Obshchei Khimii*, 1961, **31**, 840–844; (*c*) N. A. Belikova, K. V. Lebedeva, N. N. Melnikov and A. F. Plate, *Zhurnal Obshchei Khimii*, 1965, **35**, 1746–1752; (*d*) J. J. Hurst and G. H. Whitham, *J. Chem. Soc.*, 1963, 710–716; (*e*) L. I. Kasyan, N. S. Zefirov, L. Yu. Gnedenkov, N. V. Stepanova, A. S. Shashkov and E. G. Cherepanova, *Russ. J. Org. Chem.*, 1982, **18**, 1212–1218; (*f*) L. I. Kasyan, N. V. Stepanova, M. F. Galafeeva, I. E. Boldeskul, V. V. Trachevsky and N. S. Zefirov, *Russ. J. Org. Chem.*, 1987, **23**, 122–126; (*g*) L. I. Kasyan, N. S. Zefirov, N. V. Stepanova, L. E. Saltikova and O. L. Rigik, *Russ. J. Org. Chem.*, 1984, **20**, 2136–2139.

6 (*a*) M. S. Malinovsky, L. I. Kasyan, V. D. Ovsyanik, Yu. Yu. Samitov, P. B. Terentyev and A. B. Belikov, *Russ. J. Org. Chem.*, 1974, **10**, 1173; (*b*) L. I. Kasyan, S. V. Sereda, K. A. Potekhin and A. O. Kasyan, O., *Heteroat. Chem.*, 1997, **8**, 177–184; (*c*) L. I. Kasyan, S. I. Okovity and A. O. Kasyan, *Heteroat. Chem.*, 1997, **8**, 185–190; (*d*) L. I. Kasyan, I. N. Tarabara, O. A. Savel'yeva and A. O. Kasyan, *Heteroat. Chem.*, 2001, **12**, 119–130; (*e*) L. I. Kasyan, I. N. Tarabara, A. O. Kasyan, S. I. Okovytyy, A. V. Tokar, S. V. Shishkina and O. V. Shishkin, *Tetrahedron*, 2007, **63**, 1790–1797.

7 (*a*) V. Gergely, Z. Akhavin and P. Vogel, *Helv. Chim. Acta*, 1975, **58**, 871–880; (*b*) H. Chrystol, J. Coste and F. Plenat, *Bull. Soc. Chim. France.*, 1969, **11**, 3934–3939.

8 (*a*) A. P. Gray and D. E. Heitmeier, *J. Org. Chem.*, 1969, **34**, 3253–3259; (*b*) C. Le Drian and P. Vogel, *Helv. Chim. Acta*, 1987, **70**, 1703–1720; (*c*) R. A. Aitken, J. I. G. Cadogan and L. J. Gosney, *J. Chem. Soc., Perkin Trans. 1*, 1994, 927–931.

9 L. I. Kasyan, O. V. Krishchik, A. O. Kasyan and I. N. Tarabara, *Russ. J. Org. Chem.*, 2004, **40**, 1878–1879.

10 L. I. Kasyan, O. V. Krishchik, L. K. Umrikhina and A. O. Kasyan, *Bull. of Dnepropetrovsk National Univ.*, 1998, **3**, 87–90.

11 V. A. Palchikov, I. N. Tarabara and L. I. Kasyan, *Russ. J. Org. Chem.*, 2007, **43**, 779–780.

12 L. I. Kasyan, O. V. Krishchik, I. N. Tarabara, A. O. Kasyan and V. A. Palchikov, *Russ. J. Org. Chem.*, 2006, **42**, 519–526.

13 Yu. V. Zefirov, *Kristallografiya (Russian)*, 1997, **42**, 936–958.

14 H.-B. Burgi and J. D. Dunitz, *Structure correlation*, vol. 2., VCH, Weinheim, 1994, pp. 741-784.

15 M. Štrajbl, J. Florián and A. Warshel, *J. Am. Chem. Soc.*, 2000, **122**, 5354–5366.

16 (*a*) M. He, F. Zhu, D. Feng and Zh. Cai, *Chem. Phys. Lett*., 2003, **377**, 13–19; (*b*) M. He, D. Feng, F. Zhu and Zh. Cai, *J. Phys. Chem. A*, 2004, **108**, 7702–7708.

17 Ch. Zhan, D. W. Landry and R. L. Ornstein, *J. Am. Chem. Soc.*, 2000, **122**, 2621–2627.

18 (*a*) Y. Xiong and Ch. Zhan, *J. Phys. Chem. A*, 2006, **110**, 12644–12652; (*b*) Ch. Zhan and D. A. Dixon, *J. Phys. Chem. A*, 2002, **106**, 9737–9744.

19 D. Cheshmedzhieva, S. Ilieva, B. Hadjieva and B. Galabov, *J. Phys. Org. Chem.*, 2009, **22**, 619–631.

20 (*a*) E. V. Ivanova and H. M. Muchall, *J. Phys. Chem. A*, 2007, **111**, 10824–10833; (*b*) J. M. Fox, O. Dmitrenko, L. Liao and R. D. Bach, *J. Org. Chem.*, 2004, **69**, 7317–7328.

21 (*a*) K. N. Rankin and R. J. Boyd, *J. Comput. Chem.*, 2001, **22**, 1590–1597; (*b*) S. L. Boyd and R. J. Boyd, *J. Chem. Theory Comput.*, 2007, **3**, 54–61.

22 L. I. Kasyan, *Russ. J. Org. Chem.*, 1999, **35**, 661–690.

23 (*a*) X. Lopez, J. I. Mujika, G. M. Blackburn and M. Karplus, *J. Phys. Chem. A*, 2003, **107**, 2304–2315; (*b*) S. J. Weiner, U. C. Singh and P. J. Kollman, *J. Am. Chem. Soc.*, 1985, **107**, 2219–2229.

24 O. Isayev, L. Gorb and J. Leszczynski, *J. Comput. Chem.*, 2007, **28**, 1598–1609 and ref. therein.

25 G. M. Sheldrick, *SHELXTL PLUS. PC Version. A system of computer programs for the determination of crystal structure from X-ray diffraction data*. Rev.5.1., 1998.

26 M. J. Frisch, G. W. Trucks, H. B. Schlegel, G. E. Scuseria, M. A. Robb, J. R. Cheeseman, J. A. Jr. Montgomery, T. Vreven, K. N. Kudin, J. C. Burant, J. M. Millam, S. S. Iyengar, J. Tomasi, V. Barone, B. Mennucci, M. Cossi, G. Scalmani, N. Rega, G. A. Petersson, H. Nakatsuji, M. Hada, M. Ehara, K. Toyota, R. Fukuda, J. Hasegawa, M. Ishida, T. Nakajima, Y. Honda, O. Kitao, H. Nakai, M. Klene, X. Li, J. E. Knox, H. P. Hratchian, J. B. Cross, V. Bakken, C. Adamo, J. Jaramillo, R. Gomperts, R. E. Stratmann, O. Yazyev, A. J. Austin, R. Cammi, C. Pomelli, J. W. Ochterski, P. Y. Ayala, K. Morokuma, G. A. Voth, P. Salvador, J. J. Dannenberg, V. G. Zakrzewski, S. Dapprich, A. D. Daniels, M. C. Strain, O. Farkas, D. K. Malick, A. D. Rabuck, K. Raghavachari, J. B. Foresman, J. V. Ortiz, Q. Cui, A. G. Baboul, S. Clifford, J. Cioslowski, B. B. Stefanov, G. Liu, A. Liashenko, P. Piskorz, I. Komaromi, R. L. Martin, D. J. Fox, T. Keith, M. A. Al-Laham, C. Y. Peng, A. Nanayakkara, M. Challacombe, P. M. W. Gill, B. Johnson, W. Chen, M. W. Wong, C. Gonzalez, and J. A. Pople, *Gaussian 03*, revision B.05; Gaussian, Inc., Pittsburgh, PA, 2003.

27 (*a*) A. D. Becke, *J. Chem. Phys.*, 1993, **98**, 1372; (*b*) A. D. Becke, *J. Chem. Phys.*, 1993, **98**, 5648; (*c*) P. J. Stephens, F. J. Devlin, C. F. Chabalowski and M. J. Frisch, *J. Phys. Chem.*, 1994, **98**, 11623; (*d*) C. Lee, W. Yang and R. G. Parr, *Phys. Rev. B*, 1988, **37**, 785.

 This journal is © The Royal Society of Chemistry 2010

28 G. A. Petersson, T. G. Tensfeldt and J. A. Montgomery, Jr., *J. Chem. Phys.*, 1991, **94**, 6091–6101.
29 T. Clark, J. Chandrasekhar, G. W. Spitznagel and P. V. R. Schleyer, *J. Comput. Chem.*, 1983, **4**, 294–301.
30 (*a*) M. T. Cancès, B. Mennucci and J. Tomasi, *J. Chem. Phys.*, 1997, **107**, 3032–3014; (*b*) M. Cossi, V. Barone, B. Mennucci and J. Tomasi, *Chem. Phys. Lett.*, 1998, **286**, 253–260; (*c*) B. Mennucci and J. Tomasi, *J. Chem. Phys.*, 1997, **106**, 5151–5158.
31 A. P. Scott and L. Radom, *J. Phys. Chem.*, 1996, **100**, 16502–16513.
32 For conversion from 1 atm standard state to 1 mol L^{-1} standard state, the following contributions need to be added to standard enthalpy and Gibbs free energy: $-RT$, and $RT\ \ln R'T$, where R' is the value of R in L atm mol^{-1} K^{-1} (ref. 35). For a reaction with A + B = C stoichiometry (such as the addition of ethoxy anion to epoxynorbornane imide mechanism), the corrections for $\Delta H^{\ddagger}$, and $\Delta G^{\ddagger}$ are RT, and $RT\ \ln R'T$. At 298 K, the corrections amount to 0.59 and –1.90 kcal mol^{-1} for $\Delta H^{\ddagger}$ and $\Delta G^{\ddagger}$ (ref. 36).
33 D. Kosenkov, Y. Kholod, L. Gorb, O. Shishkin, D. M. Hovorun, M. Mons and J. Leszczynski, *J. Phys. Chem. B*, 2009, **113**, 6140–6150.
34 H. Eyring, J. Walter and G. Kimball, *Quantum Chemistry*, John Wiley and Sons, New York, London, Sydney, 1944.
35 S. Benson, *Thermochemical Kinetics*, Wiley, New York, 1968, p. 8.
36 A. Rastelli, M. Bagatti and R. Gandolfi, *J. Am. Chem. Soc.*, 1995, **117**, 4965–4975.